Journal of Molecular Structure 1260 (2022) 132846

Contents lists available at ScienceDirect

Journal of Molecular Structure

journal homepage: www.elsevier.com/locate/molstr

Experimental and Theoretical Vibrational Spectroscopic Investigations, DFT quantum chemical analysis, Biological activities and Molecular docking on 4,4′-Dimethoxy-2,2′-Bipyridine

Meryem Alp[a,*], Senay Yurdakul[a], Belgin Erdem[b]

[a] Department of Physics, Gazi University, Ankara, Turkey, 06560
[b] Department of Health Care Services, Ahi Evran University, Kırşehir, Turkey, 40100

ARTICLE INFO

Article history:
Received 30 November 2021
Revised 14 March 2022
Accepted 15 March 2022
Available online 16 March 2022

Keywords:
4,4′-dimethoxy-2,2′-bipyridine
DFT
Vibrational spectra
Photoluminescence
Thermodynamic properties
Antimicrobial activity and Molecular docking

ABSTRACT

The present study describes the torsional potentials, molecular geometry in monomer and dimer forms of purchased 4,4′-dimethoxy-2,2′-bipyridine (Dmobpy). The results of experimental Fourier Transform Infrared (FT-IR) and Raman (FT-RA) spectra were compared with theoretical data. Quantum chemical calculations on the optimized molecular geometries and some properties of molecules have been computed by using density functional theory (B3LYP) with basis set 6-311++G(d,p). Molecular parameters such as bond lengths, bond angles and dihedral angles were compared with X-ray diffraction data. Molecular characteristics like HOMO-LUMO energy, molecular electrostatic potential surface maps, atomic charges, Fukui functions and thermodynamic properties were investigated. This study also includes experimental photoluminescence spectrum of the title molecule. Antimicrobial study was carried out using a compound synthesized against four Gram-positive, four Gram-negative bacterias and two yeasts. We also studied docking protein interactions with the ligand molecule. The detailed studies of the molecule help in understanding structural, physical and chemical properties of further application in field of material technology.

1. Introduction

Bipyridines are one of the important class of compounds belonging to the heterocyclic azaaromatic species derived from biphenyl. The C-C bond acts as the interlink between the two pyridyl rings in a bipyridine. Thanks to their electronic structure originating from the π-bond conjugate system in the pyridyl rings and the two active nitrogen atoms, they become materials of great importance, together with metal complexes. It is known that the nitrogen rich bipyridine and its derivatives are a class of ligands that show anti-cancer, anti-fungal, anti-microbial, anti-viral, anti-inflamatory and DNA interaction activities [1,2]. Bipyridine and its derivatives have been widely used in the fields of inorganic, organometallic, electronic chemistry, medicine and also pharmaceutical field [3–5]. Because of many applications in material and medicinal chemistry, synthesis of pyridine derivatives and their different coordination complexes are important for the investigations of physicochemical properties such as catalysis, nonlinear optics and luminescence [6,7]. Metal complexes of bipyridines have interesting applications in solar energy and energy storage [8,9]. Thus, the diversification of metal compounds using ligands with biological activity is a good strategy for metal-drug development [5,10].

The aim of presenting series of vibrational spectroscopic studies on the 4,4′-dimethoxy-2,2′-bipyridine structure with the help of quantum chemical calculations in this study is that vibrational spectroscopy is an effective tool to study molecular environments, structural properties, intra- and inter-molecular interactions, bond structure and molecular vibrations. Density functional theory (DFT) calculations along with vibrational spectroscopy also have been proved to be a powerful tool to derive the various molecular properties of bioactive molecules. In the functional group analysis of drugs, These local reactivity descriptors play a vital role in the design of new pharmaceutical compounds and in understanding the between biological systems [11,12].

4,4′-dimethoxy-2,2′-bipyridine (Dmobpy) free ligand and derivatives are organic molecules of biological importance. In new drug designs, the coordination of metal and ligand used in organometallic compounds changes its chemical and medical properties. Furthermore, the ligands bearing conjugated electron-rich heteroaromatic rings, such as pyridine rings are important in

* Corresponding author.
E-mail addresses: meryem.alp@gazi.edu.tr (M. Alp), senayy@gazi.edu.tr (S. Yurdakul), berdem@ahievran.edu.tr (B. Erdem).

https://doi.org/10.1016/j.molstruc.2022.132846
0022-2860/

the understanding of electron transfer processes, mixed-valence complexes, and photochemistry. They are also used for the formation of different metal complexes including transition metals in biological processes [13–15].

Crystallographic data of 4,4′-dimethoxy-2,2′-bipyridine molecule was given by Kusano et al. [16]. Although its industrial and medical importance, the structural and vibrational spectroscopic analysis for Dmobpy were limitedly reported, and the crystal structure and vibrational spectroscopic study of pure vibrational spectroscopic molecule is still unavailable. Consequently, the review of literature signifies that the experimental and theoretical research is mainly focused on different metals complexation of various dimethoxy-bipyridine.

In this study, we reported the spectroscopic investigation of monomer and dimer forms of 4,4′-dimethoxy-2,2′-bipyridine by using B3LYP/6-311++G(d,p) level of the theory. The vibrational frequencies with total energy distributions (TEDs) data and structural parameters of the title molecule were also calculated for the most stable gas phase. HOMO-LUMO energies and quantum chemical properties were presented in the following sections. Molecular electrostatic potential, charge analysis, fukui functions, and termodynamic properties are computed and discussed. The photoluminescence properties of title molecule were experimentally performed.

Due to increasing antimicrobial resistance, new strategies have become necessary to efficiently combat pathogenic bacteria. As mentioned above, there is a growing interest in metal-based drug development. In this sense, the antimicrobial effects of 2,2-bipyridine and many metal compounds are still being investigated. Such studies are important in terms of predicting the activities of metal organic drug structures in future studies [17,18]. Therefore, the antimicrobial effects of 4,4′-dimethoxy-2,2′-bipyridine structure against bacteria such as B.thrugensisi S.auerus, which is not found in the literature, were experimentally investigated and supported by docking studies.

For this purpose, in our study, antimicrobial activity of the title compound was tested against eight bacterias and two yeasts. The compound was tested in vitro against bacterias and yeasts species *S. aureus* ATCC 29213, *B. thrungiensis* ATCC 13367, *L. monocytogenes* ATCC 35152, *P. mirabilis* ATCC 29906, *V. angilarum* ATCC43312, *E. faecalis* ATCC 29212, *E. aerogenes* ATCC 51342, *S.typhimurium* ATCC 14028, C. tropicalis ATCC M007 and C. parapsilosis ATCC M006 by microdilution method and agar well diffusion method. Lastly, the detailed investigation of the interactions between the ligand molecule and three proteins (4URM, 6KOC and 6GXS) was also evaluated with molecular docking studies.

2. Experimental Details

2.1. General

We performed the experimental IR, Raman, photoluminescence spectroscopy, and antimicrobial activity studies of the 4,4′-dimethoxy-2,2′-bipyridine that was obtained from Sigma Aldrich Chemical Company. The FT-IR spectrum of Dmobpy molecule was recorded in the range of 3500-550 cm^{-1} with Bruker Vertex 80 FT-IR spectrometer equipped with a Pike MIRacle ATR accessory. The FT-Raman spectrum was taken between 3500 and 500 cm^{-1} in a laser wavelength 532nm Jasco NRS4500 Confocal Mıcroscope Raman spectrometer with single monochromator. The photoluminescence spectrum was recorded between HORIBA JobinYvon PL system (He-Cd laser, Xenon lamp, CCD camera and liquid nitrogen cooled InGaAs dedector). FT-IR and FT-Raman samples were examined all dry and the PL sample was dissolved in ethanol.

2.2. Determination of antimicrobial and anti-quorum sensing activity by agar well diffusion method

Inoculated test bacteria were placed in Nutrient Broth (Difco) and incubated for 24-48 h. Mueller Hinton Agar (Oxoid) was used in the agar well diffusion method to count bacteria and yeast (10^6 per mL) over a 24-48-h. The culture plate wells were drilled with a sterile cork borer (7 mm diameter). Each of the synthesized compounds had a stock solution (60 mg/mL) prepared in ethyl alcohol, which was graded and diluted. Plates (Mueller Hinton Agar for bacteria and Sabouraud dextrose agar medium for yeast) were incubated for 24-48 h at 37°C (for bacteria) and 30°C (for yeast).

The inhibition zones formed on the agar plates were measured is millimeters (mm). Positive controls included ampicillin and cycloheximide, while negative controls included Etil alcohol. Each step of the disk diffusion method was carried out in accordance with the NCCLS guidelines [19].

In addition, Dmobpy1′s anti-quorum sensing activity against *C. violaceum* ATCC 12472 in LB agar was determined. A swap was used to spread a *C. violaceum* (1×10^6) culture on the LB (Luria-Bertani) agar surface. Then, using a cork borer, wells were drilled in LB agar, and the tested compound (5mg/mL) was applied to the wells after being dissolved in 10% DMSO.

The plates were incubated at 30°C for 24 hours to see if pigment production was inhibited around the well. The formation of a clear halo around the disc and the inhibition of bacterial growth were rated as positive [20].

2.3. Determination of antimicrobial activity by microdilution broth method

Minimum inhibitory concentrations (MIC) for compounds tested against bacteria and yeast strains according to the NCCLS guidelines [21]. Mueller-Hinton broth was used in bacteria suspension (0.5 McFarland), substance testing solutions (1000 g/ml in Ethyl alcohol), and MIC testing. Antimicrobial effects of synthesized compound was discovered and tested, as well as minimum inhibitory concentration (MIC) values. In 96-well microtiter plates, MIC values were determined spectrophotometrically using the microdilution broth method. For the antimicrobial effect test, 1000 µg/mL stock solution of the synthesized compound in ethyl alcohol were prepared. Bacteria and yeast stock cultures were prepared to a concentration of approximately 106 cfu/ml of bacteria and yeast, respectively, using the McFarland 0.5 turbidity standard. In 96-well plates containing 100 µL of 500, 250, 125, 62.5, 31.2, 15.6 and 7.8 µg/mL. Plates were then incubated for 24-48 hours at 37°. As a negative control, nutrient broth was used. The microorganism was present in the positive control.

2.4. Computational Details

The quantum chemical properties of 4,4′-dimethoxy-2,2′-bipyridine molecule was carried out with theoretical calculations. Density functional theory (DFT) calculations were performed with the Gaussian 09 package and molecule was visualized by using GaussView programs [22,23]. For theoretical calculations, the geometry of Dmobpy monomer and dimer structures were optimized, firstly. B3LYP functionals 6-311++G(d,p) basis set were also used to find the lowest energy optimized structure of the title molecule [24,25].

To find the lowest energy level, three different potential torsional energy calculations of the molecule were performed. These calculations include the values of the two methyl groups and pridine rings. Since the most suitable structure was chosen as the initial structure and the calculations were continued with it. The interaction energies of the dimers were calculated according to the

formula:

$$\Delta E = E_{dimer} - 2E_{monomer}$$

where E_{dimer} is the total energy of the dimer and $E_{monomer}$ is the energy of isolated Dmobpy molecule. Basis set superposition error (BSSE) was corrected by using the default counterpoise correction option implemented in Gaussian 09W package.

In this study, the DFT method (B3LYP) was used for the computation of vibrational frequencies and energies of optimized structures. The calculated vibrational frequencies of the molecules were scaled and assigned using TED (Total Energy Distribution) values. The molecular electrostatic potential (MEP) surface and the frontier molecular orbitals were visualizated by GaussView. Electronic structure parameters, charges, quantum chemical properties and thermodynamic parameters of the title compound were calculated with B3LYP/6-311++G(d,p). In order to the support the hydrogen bonding studies, fukui functions and natural bond orbital (NBO) analysis also were performed.

3. Results and Discussion

3.1. Conformational Study

For theoretical calculation, the geometry of Dmobpy monomer and dimer structures were optimized. All calculations were made in the gas phase. Geometrical optimization was made at the lowest energy level of the 4,4′-dimethoxy-2,2′-bipyridine molecule. Firstly, the torsional potential energy has been calculated as a function of the angle of rotation at intervals of 0° to 360° around the C-C pyridine interconnection. Minimum energy values of 0° have been reached for the C-C bond located between the pyridine rings and minimum energy values have been reached at 180° for the C-C bond that connects the methyl group to the pyridine ring. The bond of rotation around the O_{28}-C_{21} and O_{19}-C_{25}, which bonded methyl groups to pyridine ring have been also calculated by the same basis set. Dihedral angle C_{14}-C_{16}-O_{20}-C_{21} and C_7-C_6-O_{19}-C_{25} has varied from 0 to 360 by step of 10°. The results were presented in Fig. 1. The torsional barrier scan show the most stable geometry of the title molecule.

3.2. Monomers and Dimer Formations

We obtained two different monomers belonging to the molecular structure. One of them has the lowest energy (Dmobpy1) and the other (Dmobpy2) is the structure obtained from crystal study was carried out by Kusano [16]. However, we have seen that the energy value differ between this structure and the crystal monomer (Dmobpy2). Both structures are shown in Figs. 2 and 3, together with the numbering of the atoms. All the theoretical geometrical parameters were calculated DFT/B3LYP level of theory with the 6-311++G(d,p) basis set.

Dimer forms of 4,4′-dimethoxy-2,2′-bipyridine molecule were optimized at both 6-311++G(d,p)/3-21G levels, and corrected against BSSE (Basis Set Superposition Error). Calculated bond lenghts and bond angle parameters were given and compared with X-ray data for the monomer and dimer forms of title molecule in Table 1. The geometry of the crystal dimer structure has been taken from the study of Kusano et al. [16]. The crystal dimer has the lowest energy value (Fig. 3). As shown from Table 1 the optimized parameters were in good agreement with the experimental data. The theoretical calculations were carried out in the isolated molecule, so the environmental effects were not evaluated.

As both the monomers and the dimers are considered at the same level of theory, comparative results are predictable to be trustworthy. The minimum energy of the molecule structures are computed. The energy values are -454707.19 kcal/mol

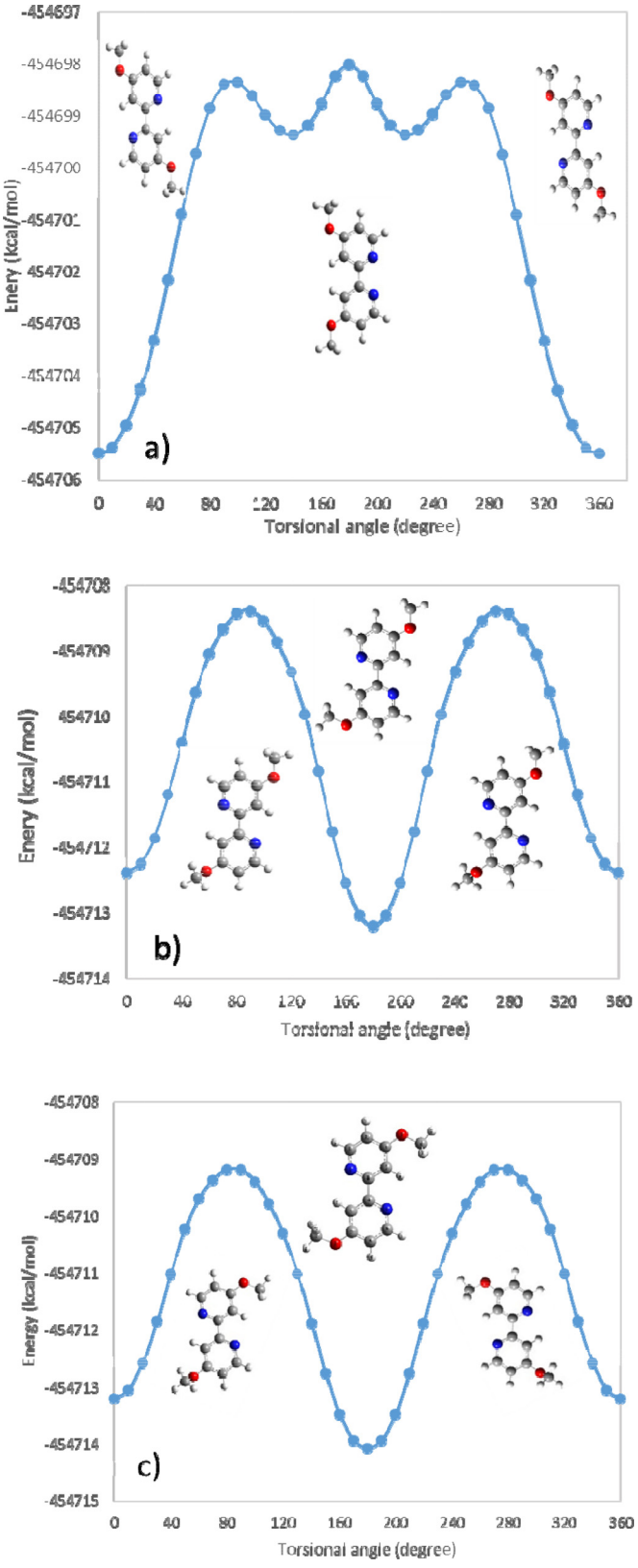

Fig. 1. The torsional barrier energy plot of Dmobpy for C-C pyridine ring and O-C methyl groups bonds a) Angles between pyridine rings are scanned b) The angles between the pyridine ring and one methyl group are scanned. c) The other methyl group angles are scanned.

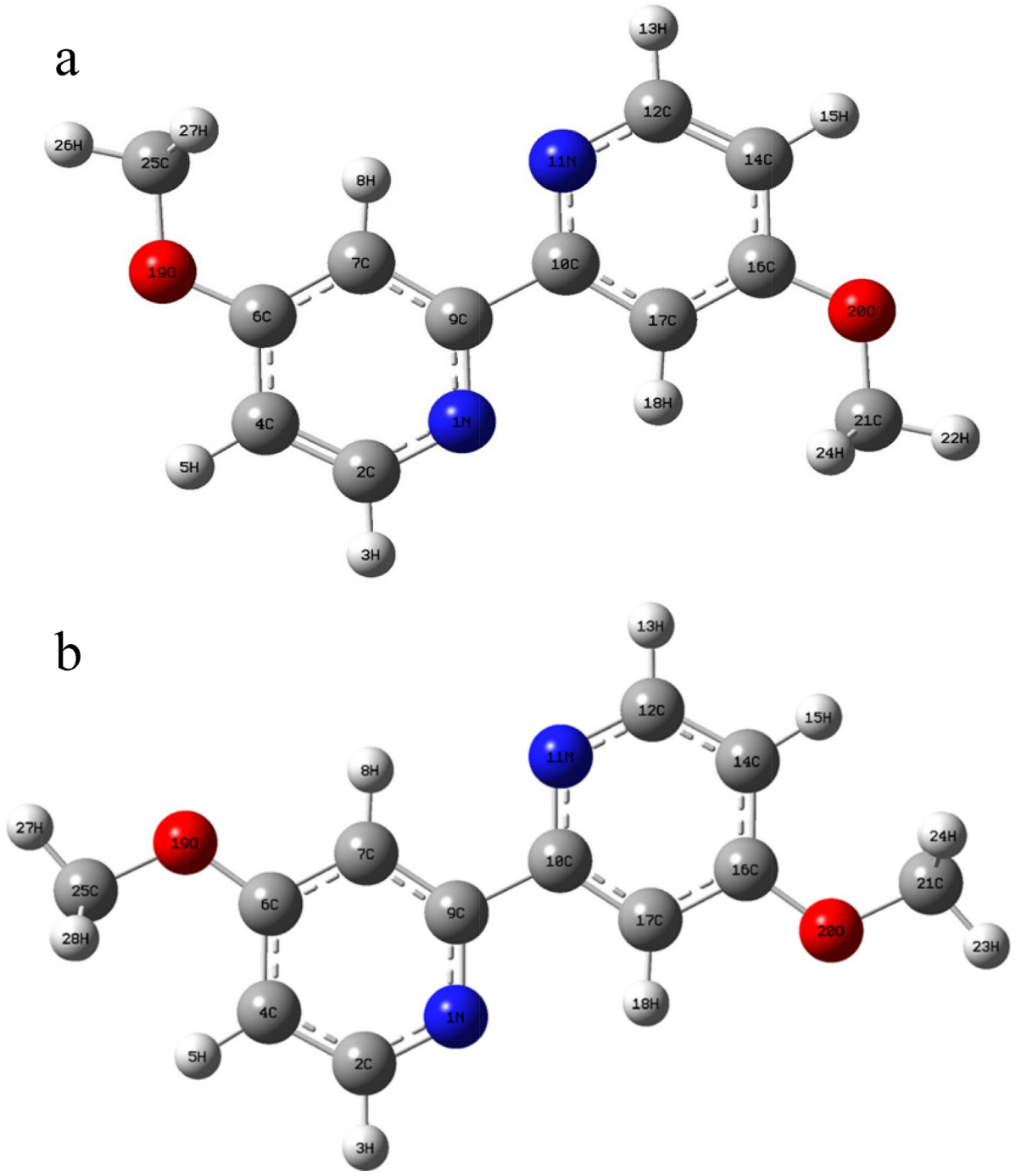

Fig. 2. Optimized molecular structure of monomer 4,4′-Dimethoxy-2,2′-Bypyridyl for a)the lowest energy level (Dmobpy1) and b) crystal monomer (Dmobpy2) at B3LYP/6-311++G(d,p) level.

(Dmobpy1), -454705.49 kcal/mol (Dmobpy2), -909413.11 kcal/mol (Dimer1) and -909415.45 kcal/mol (Dimer2), respectively. This process yielded structure of C1 symmetry for the monomers and dimers of Dmobpy. It can be observed that the difference between the minimum energy of Dmobpy1 and Dimer2 twice the energy of its monomer is -1.1 kcal/mol. Similarly, the corresponding energy difference of Dmobpy2 and Dimer1 is 2.13 kcal/mol. Counterpoise corrected binding energies (De) of dimer1 are computed as – 0.35 and -6.25 kcal/mol for both level of the basis set, respectively. Intermolecular hydrogen bond lengths are H…N=2.58 and, 2.62 Å, and H…O= 2.63 Å for the 6-311++G(d,p) level.

Consequently, the cause of deviations from experimental parameters was due to phase difference between the theoretical and experimental conditions. While some calculated values are smaller than experimental, some were larger. The largest deviation between calculated and experimental result is 0.017 Å in C10-C17 bond for Dmobpy1 and 0.012 Å in C-O bond for Dmobpy2. The calculated C-C bond lengths were close to that in the gas phase by comparison to C-N bonds. There were significant differencies in C-H bond lenghts in the Table 1. Although, the average of the C-H bond lenghts was 1.09 Å in our calculation, the experimental value was about 0.98 Å. The reason of this case is that because of the low scattering factors of hydrogen atoms in X-ray diffraction, experi-

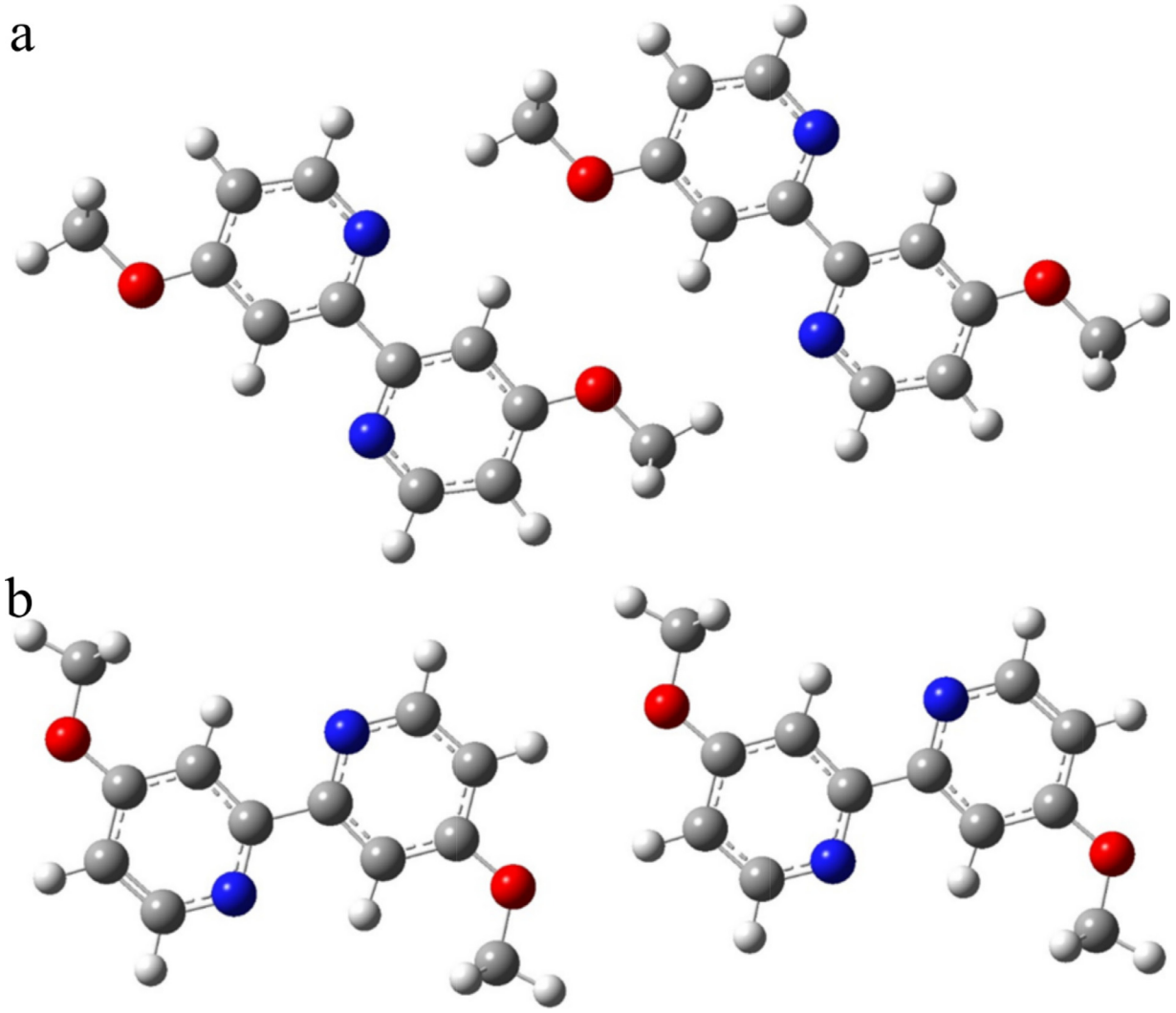

Fig. 3. Optimized molecular structure of monomer 4,4′-Dimethoxy-2,2′-Bypyridine for a)dimer1 and b)dimer2 at B3LYP/6-311++G(d,p) level.

mental bond lengths of C-H bonds are shorter than the calculated ones [16]. All remaining bond angles are very good agreement with experimental datas.

3.3. Vibrational Analysis

The Dmobpy molecule has 28 atoms, so it has 78 normal vibrational modes. It belongs to the C1 point group. All of the calculated frequencies and intensities are given in Table 2 together with experimental data. The experimental FT-IR and FT-Raman spectra of the title molecule are given in Fig. 4. In this work, theoretical calculations were carried out under the harmonic approximation by using B3LYP level with 6-311++G(d,p) basis set for the structure. The DFT/B3LYP functional tends to overestimate the fundamental modes; therefore, a scaling factor has to be used to obtain better results in agreement with experimental data. In order for the peak values to better match the experimental data, the values below 1800 cm^{-1} have multiplied by 0.970 [26] and the values above have multiplied by 0.955 cm^{-1} [27]. In addition, the highest peak value has equalized to 100 and the data were normalized. The total energy distributions (TED) were almost summarized as pure modes.

The 4,4′-dimethoxy-2,2′-bipyridine molecule's pyridine rings have six C-H stretching vibrations. The characteristic C-H stretching vibrations of the aromatic structures are in the region 3000-3100 cm^{-1} [28]. These peaks were calculated at 3088 cm^{-1}, at 3058 cm^{-1} and at 3007 cm^{-1} both in the IR and Raman spectra. These calculated vibrations were observed at 3096 and 3026 cm^{-1} in the FT-Raman spectrum and at 3065 cm^{-1} in the FT-IR spectrum (modes no.78, 74, 77). The TED contributions of pyridine rings CH vibrations were 73%, 73%, 78%, 78%, 78% and 78%, respectively. As shown in the Table 2, these values were almost the same.

The aromatic C-H vibrations of the bipyridine ring in the 4,4′-dimethyl-2,2′-bipyridine ligand were observed at 3071 and 2922 cm^{-1} [29]. These vibrations of the aromatic structures are parallel to studies of similar bipyridine based molecules [30].

The aromatic C-H in-plane bending vibrations ocur in the region 1000-1300 cm^{-1} and H out-plan bending vibrations are between 700-1000 cm^{-1}. The in-plane vibrations obtained from the FT-IR spectrum for the title molecule at 1020, 1090, 1188,1286, 1290 and 1387 cm^{-1}. 1116, 1169, 1207, and 1322 cm^{-1} in the FT-Raman spectrum. The out-plane vibrations were specified at 814/738 and 984/997 cm^{-1} in the both spectra. According to the TED analysis, the modes (υ35-υ52) especially in the range of 900 and 1300 cm^{-1} are combined with the aromatic C-H bending, υCC and υCN ring stretching vibrations. In this case, it is seen in similar aromatic compounds at the same frequency ranges [31].

Generally, stretching vibrations of methyl group are slightly lower than those of pyridine ring. The C-H stretching vibrations

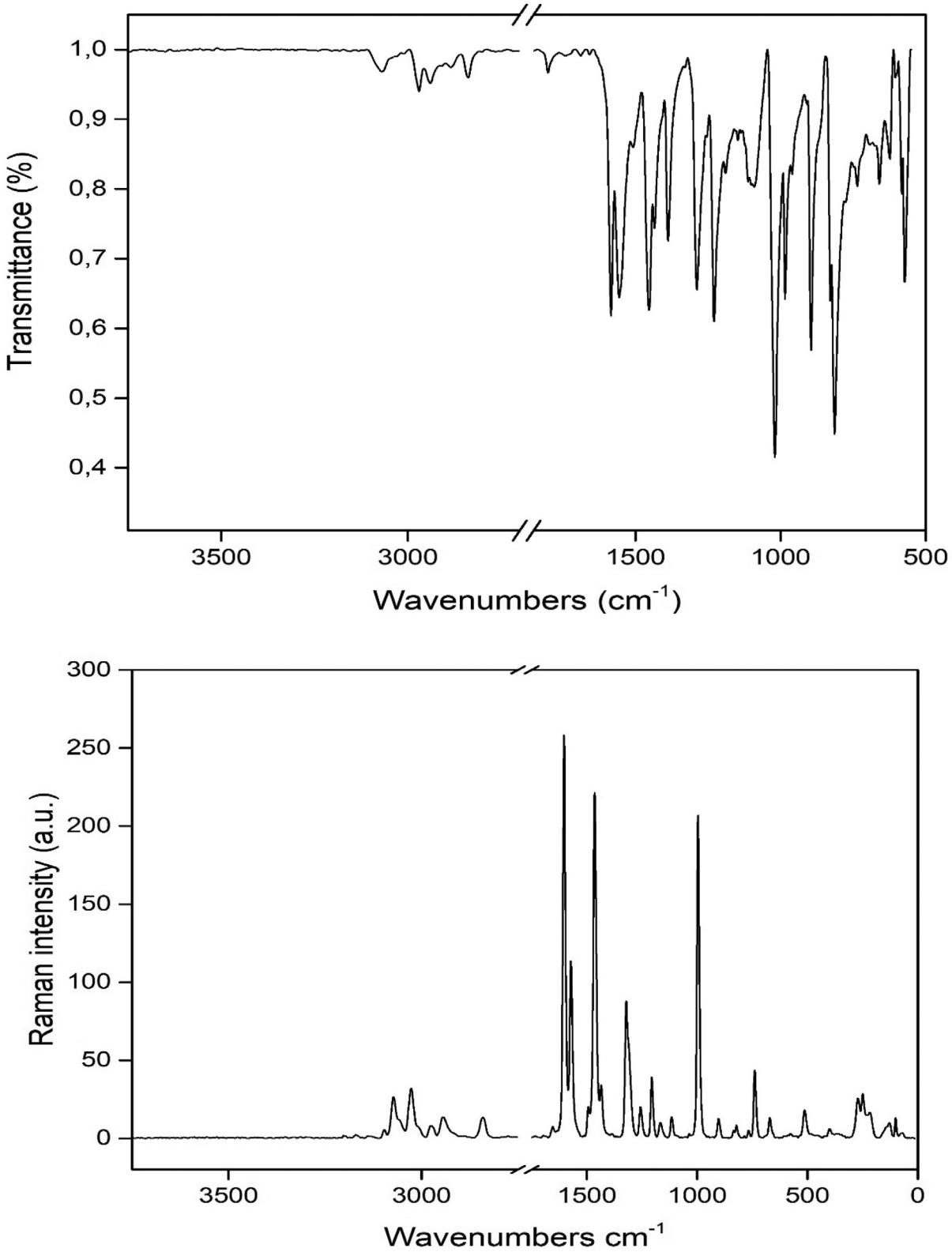

Fig. 4. Experimental Fourier Transform Infrared (a) and Fourier Transform Raman (b) spectra of Dmobpy1 which represented on the transmittance (%) against the wavenumbers (cm^{-1}), were assigned in the range of 3750-500 cm^{-1} and 3750-0 cm^{-1}, respectively.

of the methyl group were calculated at 2881 cm^{-1}, 2942 cm^{-1} and 2999 cm^{-1} . The observed peaks were at 2881/2840 cm^{-1}, 2937/2943 cm^{-1} and 2970/2976 cm^{-1} by means of FT-IR/FT-Raman spectra. The asymmetric stretching of methyl groups was assigned in the range 2942-2983 cm^{-1}, trimethylbenzene based molecules in the Ojha et al. study [32]. In the Tamer et al. study, involving metal complexes containing bipyridine and its derivatives, these stretching bands were observed in the range of 2900–3070 cm^{-1} [7].

Table 1
Calculated and experimental bond lengths and bond angles of the optimized Dmobpy1, Dmobpy2 and Dimer structures.

Bond Lenghts (Å)					
Parameters	Dmobpy1 Calc.	Dmobpy2 Calc.	Dimer1 Calc.	Dimer2 Calc.	X-Ray*
N_1-C_2	1.338	1.329	1.328	1.338	1.332
N_1-C_9	1.339	1.348	1.349	1.339	1.355
C_2-H_3	1.087	1.087	1.087	1.087	0.950
C_2-C_4	1.386	1.396	1.395	1.386	1.385
C_4-H_5	1.083	1.081	1.081	1.083	0.950
C_4-C_6	1.400	1.397	1.397	1.400	1.391
C_6-C_7	1.393	1.397	1.399	1.393	1.398
C_6-O_{19}	1.355	1.356	1.352	1.358	1.354
C_7-H_8	1.079	1.081	1.080	1.079	0.950
C_7-C_9	1.401	1.391	1.391	1.401	1.388
C_9-C_{10}	1.494	1.493	1.494	1.494	1.496
C_{10}-N_{11}	1.339	1.348	1.349	1.339	1.349
C_{10}-C_{17}	1.401	1.392	1.392	1.401	1.384
N_{11}-C_{12}	1.338	1.329	1.329	1.338	1.338
C_{12}-H_{13}	1.087	1.081	1.087	1.087	0.950
C_{12}-C_{14}	1.386	1.396	1.395	1.386	1.389
C_{14}-H_{15}	1.083	1.081	1.081	1.083	0.950
C_{14}-C_{16}	1.400	1.397	1.397	1.400	1.390
C_{16}-C_{17}	1.393	1.397	1.396	1.393	1.393
C_{16}-O_{20}	1.355	1.356	1.356	1.355	1.359
C_{17}-H_{18}	1.079	1.081	1.081	1.079	0.950
O_{19}-C_{25}	1.427	1.424	1.428	1.427	1.436
O_{20}-C_{21}	1.427	1.424	1.424	1.427	1.436
C_{21}-H_{22}	1.088	1.088	1.088	1.088	0.980
C_{21}-H_{23}	1.094	1.095	1.095	1.094	0.980
C_{21}-H_{24}	1.094	1.095	1.065	1.094	0.980
C_{25}-H_{26}	1.088	1.088	1.089	1.089	0.980
C_{25}-H_{27}	1.094	1.095	1.095	1.094	0.980
C_{25}-H_{28}	1.094	1.095	1.095	1.094	0.980
H-O				2.633	
H-O				2.633	
N-H			2.597		2,58
N-H			2.597		2,62
RMSD	0.078				
Bond Angles (°)					
Parameters	Dmobpy1 Calc.	Dmobpy2 Calc.	Dimer1 Calc.	Dimer2 Calc.	Monomer X-Ray*
C_2-N_1-C_9	117.4	117.4	117.3	117.3	116.6
N_1-C_2-H_3	116.1	116.1	115.9	115.9	117.4
N_1-C_2-C_4	124.2	124.6	124.4	124.4	125.1
H_3-C_2-C_4	119.8	119.3	119.7	119.7	117.4
C_2-C_4-H_5	121.7	119.8	121.6	121.6	121.2
C_2-C_4-C_6	118.1	117.6	117.8	117.8	117.7
H_5-C_4-C_6	120.2	122.6	120.6	120.6	121.2
C_4-C_6-C_7	118.7	118.7	118.8	118.8	118.8
C_4-C_6-O_{19}	116.6	124.9	116.7	116.7	124.6
C_7-C_6-O_{19}	124.8	116.4	124.5	124.5	116.6
C_6-C_7-H_8	123.3	120.7	123.3	123.3	120.6
C_6-C_7-C_9	118.5	118.9	118.5	118.5	118.8
H_8-C_7-C_9	118.3	120.3	118.2	118.2	120.6
N_1-C_9-C_7	123.2	122.9	123.2	123.2	123.0
N_1-C_9-C_{10}	117.1	116.9	117.2	117.2	115.8
C_7-C_9-C_{10}	119.7	120.2	119.7	119.7	121.1
C_9-C_{10}-N_{11}	117.1	116.9	117.2	117.2	116.2
C_9-C_{10}-C_{17}	119.7	120.2	119.7	119.7	120.4
N_{11}-C_{10}-C_{17}	123.2	122.8	123.2	123.2	123.4
C_{10}-N_{11}-C_{12}	117.4	117.4	117.4	117.4	116.1
N_{11}-C_{12}-H_{13}	116.1	116.1	116.0	116.0	117.4
N_{11}-C_{12}-C_{14}	124.2	124.6	124.2	124.2	125.3
H_{13}-C_{12}-C_{14}	119.8	119.3	119.8	119.8	117.4
C_{12}-C_{14}-H_{15}	121.7	119.8	121.7	121.7	121.4
C_{12}-C_{14}-C_{16}	118.1	117.6	118.1	118.1	117.2
H_{15}-C_{14}-C_{16}	120.2	122.6	120.2	120.2	121.4
C_{14}-C_{16}-C_{17}	118.7	118.7	118.6	118.6	119.0
C_{14}-C_{16}-O_{20}	116.6	124.9	116.6	116.6	125.1
C_{17}-C_{16}-O_{20}	124.9	116.4	124.8	124.8	115.9
C_{10}-C_{17}-C_{16}	118.5	119	118.5	118.5	118.9
C_{10}-C_{17}-H_{18}	118.3	120.3	118.2	118.2	120.5
C_{16}-C_{17}-H_{18}	123.3	120.7	123.3	123.3	120.5
C_6-O_{19}-C_{25}	118.5	118.6	118.4	118.4	117.5
C_{16}-O_{20}-C_{21}	118.5	118.6	118.5	118.5	117.4
O_{20}-C_{21}-H_{22}	105.6	105.7	105.6	105.6	109.5
O_{20}-C_{21}-H_{23}	111.2	111.3	111.2	111.2	109.5
O_{20}-C_{21}-H_{24}	111.2	111.3	111.2	111.2	109.5
H_{22}-C_{21}-H_{23}	109.6	109.4	109.6	109.6	109.5
H_{22}-C_{21}-H_{24}	109.6	109.6	109.6	109.6	109.5
H_{23}-C_{21}-H_{24}	109.6	109.4	109.6	109.6	109.5
O_{19}-C_{25}-H_{26}	105.7	105.7	105.8	105.8	109.5
O_{19}-C_{25}-H_{27}	111.2	111.3	111.2	111.2	109.5
O_{19}-C_{25}-H_{28}	111.2	111.3	111.2	111.2	109.5
H_{26}-C_{25}-H_{27}	109.6	109.4	109.5	109.6	109.5
H_{26}-C_{25}-H_{28}	109.6	109.6	109.5	109.5	109.5
H_{27}-C_{25}-H_{28}	109.6	109.4	109.6	109.6	109.5
RMSD	2.880				

(*continued on next page*)

Table 1 (*continued*)

* Taken from Ref [16]

The bands in the IR spectrum due to C-O stretching vibrations were observed in the region 1600 -1750 cm^{-1} [33]. The experimental peaks weren't observed at both spectra. Thomas et al. reported the C-O deformations at 1675 cm^{-1} (IR) and 1660 cm^{-1} (Raman) for experimental spectra [34].

Hence, we get eight C-C and four C-N stretching vibrations. For Dmobpy1, the modes are expected around especially 1200-1600 cm^{-1} as suggested by Ravindranath's research for bipyridine based molecules [35]. υCC and υCN ring stretching vibrations peaks were calculated at 976, 982, 1047, 1253, 1296, 1256, 1552, 1557 and 1570 cm^{-1}, respectively as consistent with same structure [29,30,35]. These peaks were observed at 984, 997, 1090, 1290, 1555, 1583 and 1603 cm^{-1} in the FT-IR and FT-Raman spectra.

Computed modes of Dmobpy dimer compared with the experimental FT-IR spectrum. Several computed N…H bands like 661, 812, 1512, and 1656 cm^{-1} are in match with the experimental data 659, 812, 1518, and 1659 cm^{-1}. Despite those matches between the computed vibrational data and experiment, it is not possible to do a complete assignment of vibrational modes by depending solely on the computed data. Hence, due to the existence of several thick bands in the experimental spectrum and the partial match between dimer forms' calculated data with experiment, we have concluded that both monomer and dimer forms of Dmobpy might exist in the sample.

The asymmetric and symmetric bending vibrations of methyl groups normally appear in the region 1465–1440 and 1390–1370 cm^{-1}, respectively [36]. The theoretical band was predicted at 1429-1460 cm^{-1} range by B3LYP/6-311++G(d,p) level of theory. In the present study, asymmetric CH_3 bending vibrations were detected at 1433-1452 cm^{-1} in the FT-IR and 1434 cm^{-1} in the FT-Raman spectra. The asymmetric CH_3 bending mode of the methyl group was also predicted at 1429 and 1448 cm^{-1} at the calculated frequencies, respectively. The symmetric C-H vibration of the CH_3 group is observed at 1387 cm^{-1} at FT-IR spectrum. This frequency was calculated at 1360 cm^{-1}. Symmetric and asymmetric bending vibrations of methyl groups belonging to similar structures were both calculated and observed at close values. In the analysis of the 7-methylcoumarin molecule, the symmetric CH_3 vibration was calculated at 1370 cm^{-1} [37]. Bending vibrations of a single methyl group were predicted at 1446-1367 cm^{-1} and also observed at 1423-1359 cm^{-1} for 4-acetylpyridine molecule [38].

The vibrational assignments of C-H stretching vibrations, ring or substituent sensitive modes, ring torsions, C-H out-of-plane bending vibrations, vibrations associated with the inter-ring C-C bond are made unambiguously using TED and eigen vectors obtained in the DFT computation, whereas the vibrational assignments of two

Table 2
Calculated vibrational wavenumbers. frequencies. scaled frequencies. normalized absorption intensities and experimental values of the infrared and Raman spectrum also their detailed assignments with total energy distribution(%) for Dmobpy1.

	Calculated				Observed				
Mod	Freq	Freq*	I_{IR}**	I_{RA}**	Freq FT-IR	I_{FT-IR}**	Freq FT-RA	I_{FT-RA}**	TED %***
υ_1	26	**25.5**	0.1	0.0			-		20 Γ_{CCCC} + 26 Γ_{NCCC} + 12Γ_{NCCN}
υ_2	84	**81.3**	0.0	0.0	-		-		12 Γ_{HCCC} + 14 Γ_{CNCC} + 21 Γ_{CCOC} + 17 Γ_{CCCC} + 13 Γ_{COCH}
υ_3	96	**93.2**	0.1	0.0			-		24 δ_{CCC} + 16 δ_{CCO} + 19 δ_{NCC}
υ_4	99	**96.3**	0.0	15.2	-		100	5.1	42 Γ_{CCOC} + 34 Γ_{COCH}
υ_5	110	**106.5**	0.1	0.0			-		10 Γ_{NCCC} + 15 Γ_{CCOC} + 27 Γ_{COCH}
υ_6	169	**164.2**	0.0	25.2	-				17 υ_{CC} + 27 δ_{CCO} + 12 δ_{CCC} + 13 δ_{COC}
υ_7	187	**181.2**	0.0	7.5	-				34 Γ_{COCH} + 11 Γ_{CCCC} + 15 Γ_{CCCO}
υ_8	204	**197.8**	0.1	0.0			-		12 Γ_{CCCO} + 38 Γ_{COCH}
υ_9	242	**234.9**	0.0	18.5	-		217	6	11 Γ_{COCH} + 11 Γ_{CCOC} + 13 Γ_{CCCC} + 13 Γ_{HCCC} + 15 Γ_{CNCC} + 13 Γ_{CCCN}
υ_10	260	**252.1**	0.0	1.4	-		270	10	14 Γ_{CCCO} + 43 Γ_{CCOC}
υ_11	266	**257.5**	0.3	0.0			-		13 Γ_{CCCO} + 36 Γ_{COCH}
υ_12	277	**268.2**	0.2	0.0			-		23 δ_{CCO} + 16 δ_{CCC}
υ_13	323	**313.0**	0.0	1.0	-				16 υ_{CC} + 18 δ_{NCC} + 15 δ_{CCC} + 12 δ_{HCC}
υ_14	431	**417.9**	0.0	14.1	-				21 υ_{CC} + 14 δ_{COC} + 18 δ_{CCC} + 12 δ_{HCC} + 11 δ_{NCC}
υ_15	433	**419.7**	0.2	0.0			-		21 Γ_{NCCC} + 13 Γ_{CCCC} + 13 Γ_{CNCC} + 13 Γ_{HCCC} + 11 Γ_{CCCO}
υ_16	465	**450.6**	0.0	0.0	-		-		10 υ_{OC} + 20 δ_{CCC} + 18 δ_{CCO} + 17 δ_{HCC}
υ_17	468	**454.1**	0.0	7.8	-				24 δ_{CCC} + 15 δ_{HCC} + 13 δ_{CCO} + 12 δ_{NCC} + 10 υ_{CC} + 10 υ_{OC}
υ_18	489	**474.4**	0.0	0.7	-				20 Γ_{CNCC} + 19 Γ_{NCCC} + 14 Γ_{HCCC}
υ_19	561	**544.0**	0.2	0.0			-		14 δ_{CCC} + 12 δ_{COC} + 17 δ_{CCH} + 11 δ_{CCO}
υ_20	585	**567.5**	0.0	4.4	-				21 δ_{CCC} + 12 δ_{CCO} + 10 δ_{COC} + 16 δ_{HCC} + 10 δ_{NCC}
υ_21	590	**572.6**	0.3	0.0	571.9	66.7	-		12 Γ_{CNCC} + 12 Γ_{COCH} + 11 Γ_{CCCO} + 11 Γ_{CCCC} + 17 Γ_{HCCC}
υ_22	680	**659.3**	0.2	0.0	659.2	86	-		26 δ_{CCC} + 25 δ_{NCC} + 25 δ_{HCC}
υ_23	680	**659.8**	0.0	1.6	-		670	5	21 Γ_{HCCC} + 16 Γ_{CCCC} + 10 Γ_{COCH} + 13 Γ_{CCOC}
υ_24	743	**720.4**	0.0	12.6	-		738	17	11 υ_{CC} + 18 δ_{CCC} + 15 δ_{NCC} + 21 δ_{HCC}
υ_25	750	**727.4**	0.0	0.0	733	81	-		18 Γ_{NCCC} + 17 Γ_{CNCC} + 13 Γ_{CCCC} + 15 Γ_{CCCH}
υ_26	787	**763.3**	0.0	0.9	-				19 Γ_{CNCC} + 27 Γ_{NCCC} + 11 Γ_{NCCH} + 12 Γ_{HCCC}
υ_27	838	**813.2**	3.4	0.0	814	45	-		12 υ_{CC} + 17 υ_{CO} + 11 δ_{CNC} + 17 δ_{NCC} + 12 δ_{HCC}
υ_28	844	**818.3**	1.9	0.0	827	65	-		14 Γ_{NCCH} + 19 Γ_{HCCO} + 24 Γ_{HCCC}
υ_29	846	**820.4**	0.0	0.6	-		825	2	14 Γ_{NCCH} + 16 Γ_{HCCO} + 24 Γ_{HCCC}
υ_30	897	**869.7**	1.1	0.0	895	57	-		33 Γ_{HCCC} + 18 Γ_{OCCH} + 15 Γ_{NCCC} + 10 Γ_{CCCC}
υ_31	915	**887.6**	0.0	0.02	-		904	5	18 Γ_{OCCH} + 19 Γ_{NCCC} + 30 Γ_{HCCC}
υ_32	946	**917.8**	0.0	3.1	-				17 υ_{CC} + 15 υ_{CO} + 15 δ_{HCC}
υ_33	981	**951.1**	0.0	0.0	-		-		14 Γ_{CNCH} + 25 Γ_{HCCH} + 21 Γ_{HCCC}
υ_34	982	**952.2**	0.0	0.3	-				14 Γ_{CNCH} + 23 Γ_{HCCH} + 24 Γ_{HCCC}
υ_35	1006	**976.1**	0.3	0.0	984	64	-		11 υ_{CN} + 18 υ_{CC} + 13 δ_{HCC} + 15 δ_{NCC} + 20 δ_{CCC}
υ_36	1013	**982.3**	0.0	63.5	-		997	77	10 υ_{CN} + 19 υ_{CC} + 15 δ_{HCC} + 15 δ_{NCC} + 21 δ_{CCC}
υ_37	1055	**1023.6**	5.0	0.0	1020	42	-		23 υ_{OC} + 10 δ_{HCC} + 11 δ_{NCC} + 13 δ_{CCC}
υ_38	1059	**1026.8**	0.0	1.2	-				15 υ_{CC} + 19 υ_{CO} + 24 δ_{HCC}
υ_39	1079	**1047.1**	0.2	0.0			-		15 υ_{CC} + 11 υ_{CN} + 42 δ_{HCC}
υ_40	1110	**1076.4**	0.0	5.9	-		1116	1	15 υ_{CC} + 50 δ_{HCC}
υ_41	1125	**1091.4**	0.0	0.0	1090	80	-		15 υ_{CC} + 51 δ_{HCC}
υ_42	1168	**1132.8**	0.0	1.5			1169	0.2	18 δ_{OCH} + 12 δ_{HCH} + 28 Γ_{COCH} + 10 Γ_{CCOC}
υ_43	1168	**1132.8**	0.0	0.1	1145	87			18 δ_{OCH} + 12 δ_{HCH} + 28 Γ_{COCH} + 10 Γ_{CCOC}
υ_44	1187	**1151.4**	0.0	8.6	-				10 υ_{CO} + 16 δ_{OCH} + 34 δ_{HCC}
υ_45	1203	**1167.0**	0.0	0.0	1188	82	-		11 δ_{HCC} + 34 δ_{OCH} + 12 δ_{HCH} + 20 Γ_{COCH}
υ_46	1218	**1181.3**	0.0	22.6	-		1207	14	16 δ_{HCC} + 24 δ_{OCH} + 11 δ_{HCH} + 14 Γ_{COCH}
υ_47	1274	**1236.1**	9.0	0.0			-		12 υ_{CO} + 28 δ_{HCC}
υ_48	1293	**1253.7**	0.0	2.5	-				19 υ_{CN} + 26 υ_{CC} + 16 δ_{CCH}
υ_49	1295	**1256.4**	2.6	0.0	1286		-		10 υ_{CO} + 13 υ_{NC} + 21 υ_{CC} + 19 δ_{HCC}
υ_50	1329	**1288.8**	0.0	7.1	-				14 δ_{NCH} + 39 δ_{CCH}
υ_51	1336	**1296.0**	5.4	0.0	1290	66	-		10 υ_{CO} + 15 υ_{NC} + 18 υ_{CC} + 18 δ_{HCC}
υ_52	1347	**1306.5**	0.0	76.7	-		1322	33	10 υ_{CO} + 16 υ_{CC} + 17 δ_{HCC} + 14 δ_{CCC}
υ_53	1401	**1359.3**	0.6	0.0	1387	73	-		14 υ_{CC} + 38 δ_{HCC}
υ_54	1453	**1409.7**	0.0	31.6	-		1434	13	18 υ_{CC} + 16 δ_{HCH} + 16 δ_{OCH} + 18 δ_{CCH}
υ_55	1473	**1428.6**	2.8	0.0	1433	75	-		26 δ_{HCH} + 27 δ_{OCH} + 21 δ_{CCH}
υ_56	1486	**1441.5**	0.0	37.1	-				22 δ_{HCH} + 22 δ_{OCH} + 16 δ_{CCH}
υ_57	1493	**1448.4**	0.6	0.0	1452	91	-		48 δ_{HCH} + 11 δ_{OCH} + 35 Γ_{COCH}
υ_58	1493	**1448.4**	0.0	5.9					48 δ_{HCH} + 11 δ_{OCH} + 35 Γ_{COCH}
υ_59	1501	**1456.2**	6.2	0.0			-		27 δ_{HCH} + 41 δ_{CCH} + 13 Γ_{COCH}
υ_60	1504	**1459.2**	0.0	5.3	-		1493	8	12 δ_{OCH} + 42 δ_{HCH} + 22 Γ_{COCH}
υ_61	1505	**1459.7**	0.4	0.0	1504	88	-		16 δ_{HCC} + 11 δ_{OCH} + 28 δ_{HCH} + 16 Γ_{COCH}
υ_62	1521	**1475.6**	0.0	4.3	-				13 υ_{CC} + 10 δ_{NCH} + 32 δ_{HCC}
υ_63	1600	**1552.4**	5.3	0.0	1558	65	-		13 υ_{CN} + 25 υ_{CC} + 24 δ_{HCC} + 12 δ_{CCC}
υ_64	1606	**1557.3**	0.0	100	-		1603	100	14 υ_{CN} + 23 υ_{CC} + 20 δ_{HCC} + 13 δ_{CCC}
υ_65	1620	**1570.9**	18.6	0.0	1583	62	-		10 υ_{CN} + 19 υ_{CC} + 30 δ_{HCC}
υ_66	1632	**1583.1**	0.0	36.1	-		1624	3	23 υ_{CC} + 26 δ_{HCC}
υ_67	3017	**2881.5**	100.0	14.7	2837	96	2840	5	90 υ_{CH} (methyl)
υ_68	3017	**2881.5**	2.4	0.1	2881	97			90 υ_{CH} (methyl)
υ_69	3081	**2942.2**	0.0	3.5			2943	5	81 υ_{CH} (methyl)
υ_70	3081	**2942.3**	1.8	0.02	2937	95			81 υ_{CH} (methyl)
υ_71	3141	**2999.2**	1.4	0.0	2970	94	-		81 υ_{CH} (methyl)
υ_72	3141	**2999.2**	0.0	12.4	-		2976	3	80 υ_{CH} (methyl)
υ_73	3148	**3006.5**	1.8	0.0					78 υ_{CH} (py)
υ_74	3148	**3006.7**	0.0	11.4			3026	12	78 υ_{CH} (py)
υ_75	3202	**3057.6**	0.3	0.0			-		79 υ_{CH} (py)
υ_76	3202	**3057.7**	0.0	15.2	-				78 υ_{CH} (py)
υ_77	3233	**3087.7**	0.4	0.0	3065	97	-		73 υ_{CH} (py)
υ_78	3234	**3088.2**	0.0	2.4	-		3096	2	73 υ_{CH} (py)

* Scaled wavenumbers calculated at B3LYP/ 6-311 G++(d.p) using scaling factors 0.997 for the wavenumber less than 1800 cm^{-1}[26] and 0.955 above 1800 cm^{-1}[27].

** Relative absorption intensities and relative Raman intensities normalized with highest peak absorption equal to 100.

*** Total energy distribution calculated B3LYP 6-311++G(d.p) level. TED less than 10% are not shown.

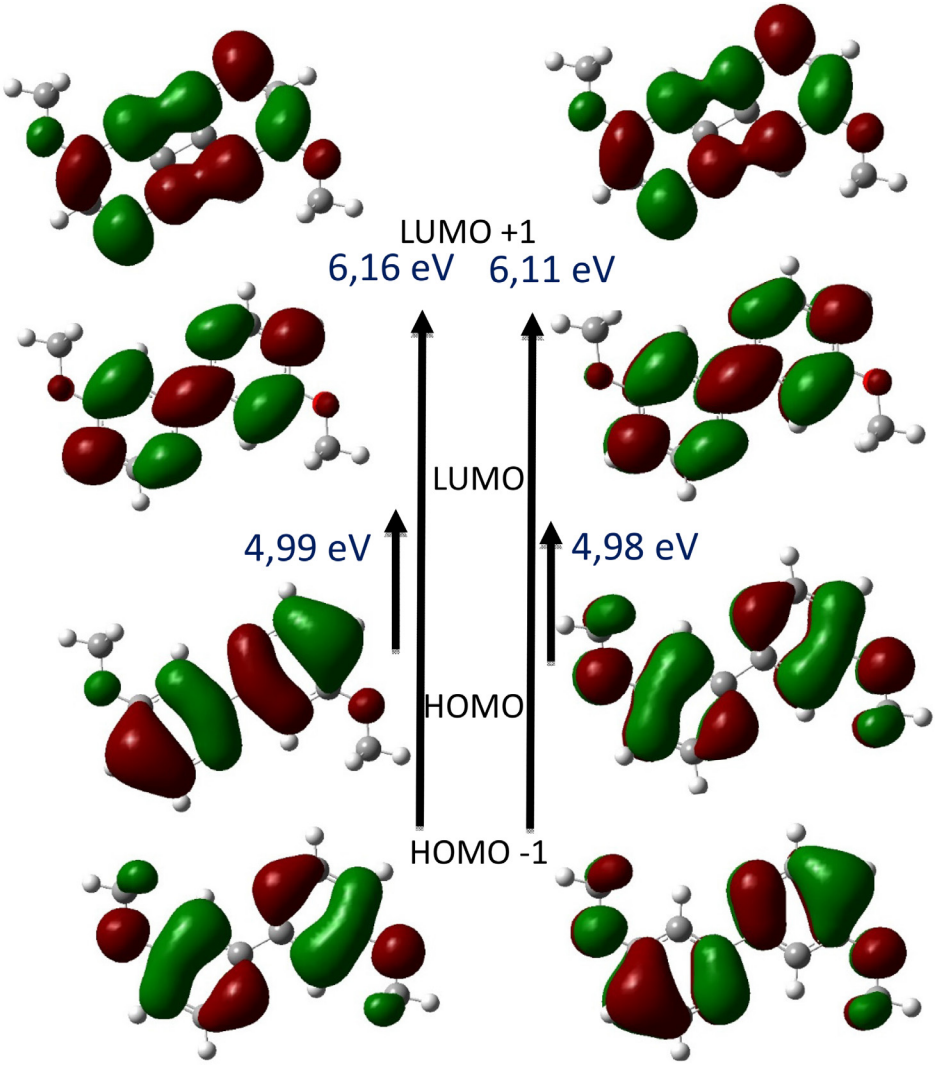

Fig. 5. The calculated energy values of the molecular orbitals of the Dmobpy1 molecule.

methyl groups are made on the same lines as presented in Ojha et al. [32].

3.4. Frontier Molecular Orbital Analysis

The highest occupied molecular orbital (HOMO) and lowest unoccupied molecular orbital (LUMO) are the orbitals which denote the chemical stability of the molecule. The HOMO, which indicates the ability to donate an electron and LUMO, shows the ability to accept an electron. Their energy gives an information about directly related to the ionization potential and the electron affinity [39]. HOMO-LUMO energy gap is a measure of molecular chemical reactivity. The smaller energy gap means that the molecule is more reactive [40]. The calculated band gap energy of the Dmobpy1 is 4.99 eV. The relatively high value of HOMO-LUMO indicates that the compound has high chemical stability and low reactivity. It has also been determined to be more stable than the oxygen-free structure in the work of Ravindranath et al. [35]. In addition to, it can be said that the Dmobpy is more polarizable than the urea because its energy gap is lower than the urea (ΔE_{urea}= 6.7063 eV) [41].

As seen from Fig. 5, the HOMO levels are spread over the entire molecule, except methyl groups in the ground state. The LUMO of the first excited state also shows a similar distribution. The calculated energies of the orbitals and some quantum chemical properties of the compound were summarized in Table 3. The ionization energy (**I**), electron affinity (**A**), global hardness (η), chemical potential (μ_c), softness (σ) and global electrophilicity (ω) are calculated by using by the energy band gap value. The relevant expressions are;

$I = -E_{HOMO}$, $A = -E_{LUMO}$, $\eta = (-E_{HOMO} + E_{LUMO})/2$, $\mu = (E_{HOMO} + E_{LUMO})/2$ and $\omega = \mu^2 / 2\eta$ [42].

These parameters are useful for determining various aspects of their pharmacological structure, including drug design and toxicological properties of drug molecule [43]. The ionization energy (**I**) and electron affinity (**A**) are calculated to be 6.59 eV, and 1.60 eV, respectively. Chemical hardness of the Dmobpy1 is 2.50 eV, so we can define the molecule as hard and stable. Also, the calculated electrophilicity (ω) value is 3.37 eV. For the $\omega > 1.5$ eV, the organic molecule is considered as strong molecule [44]. The biological activity of molecules can be described using the electrophilicity index. Dmobpy value showed that the molecule is biologically active [45].

Ground-state dipole moment is an important factor in measuring solvent effects, a large one gives rise to a strong solvent polarity effect. Solvent effects can change the charge displacement

Table 3
The energy band gaps and quantum chemical properties of the Dmobpy1 at DFT/B3LYP/6-311++G(d,p).

Molecular Orbitals	Energy (eV)			Energy gap (eV)		Ionization potential (I) (eV)		Electron affinity (A) (eV)		Global hardness (η) (eV)		Electronegativity (χ) (eV)		Chemical potential (μ_c) (eV)		Global softness (σ) (eV^{-1})		Global electrophilicity (ω) (eV)	
	Gas	EtOH		Gas	EtOH	Gas	EtOH	Gas	EtOH	Gas	EtOH	Gas	EtOH	Gas	EtOH	Gas	EtOH	Gas	EtOH
H	-6.59	-6.80	ΔE_{H-L}	4.99	4.98	6.59	6.8	1.60	1.82	2.50	2.49	4.10	4.31	-4.10	-4.31	0.20	0.20	3.37	3.73
L	-1.60	-1.82																	
H-1	-6.89	-7.05	$\Delta E_{H-1-L+1}$	6.16	6.11	6.89	7.05	0.73	0.94	3.08	3.05	3.81	4.00	-3.81	-4.00	0.16	0.16	2.36	2.62
L+1	-0.73	-0.94																	
H-2	-7.07	-7.28	$\Delta E_{H-2-L+2}$	6.81	6.81	7.07	7.28	0.26	0.47	3.40	3.40	3.66	3.88	-3.66	-3.88	0.15	0.15	1.97	2.21
L+2	-0.26	-0.47																	

H: HOMO(Highest Occupied Molecular Orbital); L: LUMO(Lowest Unoccupied Molecular Orbital); eV: electronVolt; eV^{-1}: 1/electronVolt.

in molecules. Thus, the dipole moment of the system is induced and can increase, indicating a relationship with solvent energies, dielectric constants or dipole moments.

We have also investigated Dmobpy1 molecular orbital analysis when it is solvated in ethanol. The solvation energy(ΔE_s), solvation free energy(ΔG_s) and dipole moments of Dmobpy1 in the solution predicted at B3LYP/6-311++G(d,p) level of theory. The calculated data are tabulated and compared with the gas phase values on Table 3. The solvent effects have been taken into account based on the polarizable continuum model (PCM) [46].

We obtained the same dipole moment values in gas phase and EtOH solution, 0.0001 debye (Dmobpy1). This value shows us that the molecule has a stable structure and that the solvent interaction is weak. Since the energy band gap values of the molecule did not change in the ethanol solution, no change was observed in the global hardness and softness values.

The solvation-free energy, ΔG_s, is the work needed to transfer molecules from the gas phase into the solution. It plays a significant role in the understanding of the chemical characterization of molecules in the condensed phases. solvation-free energy is considered a key molecular characteristic in drug discovery studies [47]. The relevant expressions are;

$$\Delta E_s = E_{solution} - E_{gas}, \quad \Delta G_s = G_{solution} - G_{gas}$$

The calculated values are ΔG_s = -2,31044, and ΔE_s = 0 kJ/mol.

The density of states (DOS) plots is generally used to calculate the band structure. The DOS spectrum was created by convoluting the molecular orbital information with Gaussian curves of unit height. The DOS analysis was obtained with the GaussSum 3.0 program, developed by O'Boyle et al. It can be noticed from the figure the numbers of orbitals and their energy level [48]. The green lines in the DOS spectrum indicate the HOMO levels and the blue ones LUMO levels (Fig. 6). In Dmobpy, both the HOMO and the LUMO are mainly localized on the whole molecule.

3.5. Molecular Electrostatic Potential and Charge Analysis

The molecular electrostatic potential surface (MEP) is a exceptionally useful method to estimate the molecular interactions, chemical reactivity and hydrogen bonding of the stucture [49]. MEP surface has calculated by B3LYP/6-311++G(d,p) basis set and present in Fig. 7. The maximum negative and positive potentials were calculated as – 3.25e-2 a.u.(deepest red) and 3,25e-2 a.u. (deepest blue). The region around the nitrogen and oxygen atoms was found to be electron rich (red). The MEP is best suited for identifying sites for intra and intermolecular interactions [50]. The red color refers to the electron rich nucleophilic regions, as blue color refers to the electrophilic regions. As for the positive region, the hydrogen atoms of methyl groups have the highest positive potential [29].

The bond ability of atoms were investigated by calculating the charge distributions of the optimized structure. Effective charge density calculations play an important role in quantum chemical calculations of molecular systems, since atomic charges affect the dipole moment, molecular polarizability, electronic structure, acidic-basic behavior and many other properties of molecular systems. The electronic charges of atoms define the binding potential of a molecule.

The charges of each atom have been calculated in three different ways. These are Natural Bond Orbital analysis, Atomic Polar Tensor and Hirshfeld load analysis. In the Natural Bond Orbital analysis, the orbitals are orthogonalized and localized to form one or two center orbitals. These orbitals are classified as core orbitals. Hirshfeld atomic charge analysis based on electron density; The charge of each atom is obtained by integrating the electron

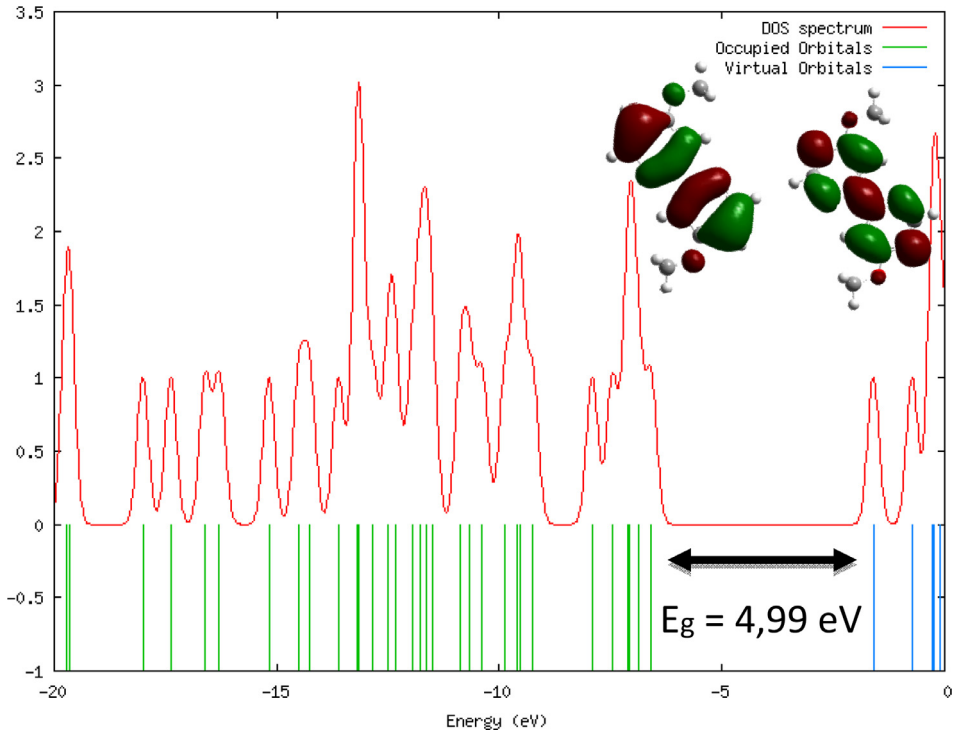

Fig. 6. Density of states (DOS) diagram for Dmobpy1 in the gas phase.

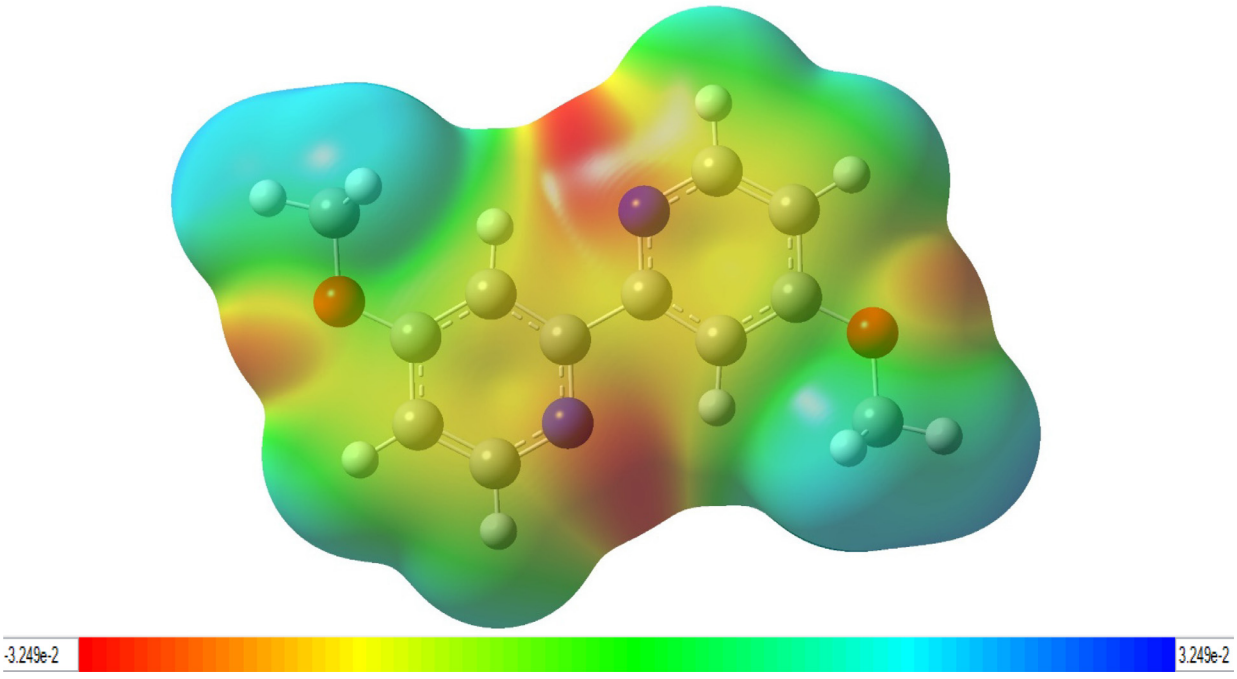

Fig. 7. Molecular electrostatic potential for the title molecule (Dmobpy1) in gas phase.

density volume. Atomic Polar Tensor analysis is defined using the atomic polar tensor of a molecule [51,52]. The charge values of the molecule are given in Table 4 and also Fig. 8. The negative charge values observed in N_1, C_4, C_7, N_{11}, C_{14}, C_{17}, O_{19} and O_{20} also the remaining atoms are positively charged.

3.6. Fukui Functions

In Fukui's Frontier Molecular Orbital Theory, the chemical reactivity of the molecule is evaluated in terms of HOMO or LUMO electron density. Fukui functions were calculated by using the finite difference (FD) methodology for the neutral cationic and anionic structure of the optimized geometric structure. In FD calculations, three types of Fukui functions have been defined [53].

$$f_k^+ = q_k(N+1) - q_k(N) \text{ for nucleophilicity,} \quad (1)$$

$$f_k^- = q_k(N) - q_k(N-1) \text{ for electrophilicity,} \quad (2)$$

$$f_k^0 = (1/2)\,[q_k(N+1) - q_k(N-1)] \text{ for neutrality,} \quad (3)$$

Table 4
Atomic charge values of the Dmobpy1 molecule (APT, NBO, Hirshfeld).

Atom	APT	NBO	Hirshfeld	Atom	APT	NBO	Hirshfeld
N_1	-0.539	-0.494	-0.161	H_{15}	0.060	0.223	0.050
C_2	0.262	0.068	0.017	C_{16}	0.831	0.357	0.088
H_3	0.009	0.185	0.042	C_{17}	-0.379	-0.311	-0.072
C_4	-0.268	-0.278	-0.065	H_{18}	0.115	0.245	0.034
H_5	0.060	0.223	0.050	O_{19}	-0.917	-0.534	-0.130
C_6	0.831	0.357	0.088	O_{20}	-0.917	-0.534	-0.130
C_7	-0.378	-0.304	-0.072	C_{21}	0.483	-0.207	0.007
H_8	0.115	0.245	0.034	H_{22}	0.003	0.192	0.051
C_9	0.380	0.193	0.053	H_{23}	-0.020	0.175	0.043
C_{10}	0.380	0.212	0.053	H_{24}	-0.020	0.175	0.043
N_{11}	-0.539	-0.497	-0.161	C_{25}	0.483	-0.207	0.007
C_{12}	0.262	0.068	0.017	H_{26}	0.003	0.192	0.051
H_{13}	0.009	0.185	0.042	H_{27}	-0.020	0.175	0.043
C_{14}	-0.267	-0.278	-0.065	H_{28}	-0.020	0.175	0.043

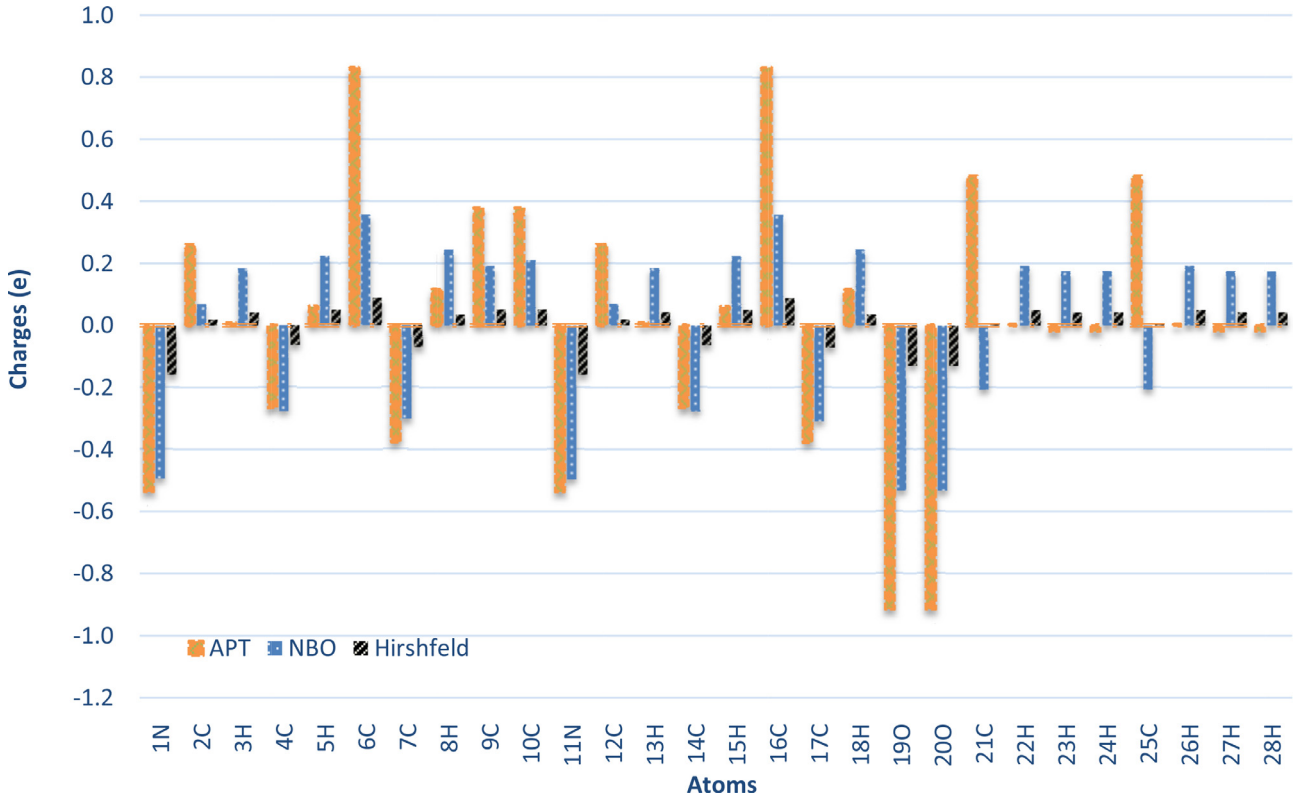

Fig. 8. Electronic charge distribution (APT, NBO and Hirshfeld) for the Dmobpy1 molecule.

In these equations, q_k represents the atomic charges in neutral (N), anionic (N+1) and cationic (N-1) states in the atomic region [54,55]. The chemical reactivity of atoms was interpreted by proportioning the f^+ and f^- values obtained as a result of calculations to each other. If the high value belongs to the (f^+/f^-) ratio, the atom is expected to show electrophilic properties, and the atom to be nucleophilic if the (f^-/f^+) ratio [55,56]. While the maximum value of electrophilic reactivity identifiers was determined in the O_{19} and O_{20} atoms for the Dmobpy1 molecule, the maximum value of the nucleophilic reactivity identifiers was observed in the C_{10} atom. Based on these results, we predict the atoms of the molecule that are likely to react (Table 5).

3.7. Thermodynamic Properties

Thermodynamic functions were obtained by 6-311G++(d,p) basis set vibration analysis of molecules in the gas phase. On the basis of vibration analysis, static thermodynamic functions: heat capacity (Cp), entropy (S), enthalpy changes (ΔH) and Gibbs free energy (G) for the title molecule derived from theoretical thermodynamic parameters are also listed in the Table 6. It is known that these properties play an important role in the characterization of the material and are important for understanding the environmental effects and reactivity on the molecules. Thermodynamic data reveals useful information on the compounds studied when they are viewed as a reactant involved in a new reaction. Since the molecule is a characteristic feature, the zero point vibration energy remains constant at all temperatures. The zero-point vibration energy obtained for the optimization of the ligand was calculated as 0.22 a.u. for the Dmobpy1. Apparently, all of the thermodynamic parameters analyzed show an increase in the same direction as temperature, but G has been observed to decrease with T due to the rise in temperature and molecular vibrations. Entropy and enthalpy changes show that the molecule has more flexibility in changing its thermodynamic system by temperature. They can be used to estimate the directions of chemical reactions in accor-

Table 5
Calculated Fukui functions values of the Dmobpy1 molecule from Hirshfeld charges.

Atom	-1	0	+1	f+	f-	f0	f+/f-	f-/f+
N_1	-0.206	-0.161	-0.108	0.053	0.045	0.049	1.175	0.851
C_2	-0.025	0.017	0.055	0.037	0.043	0.040	0.871	1.149
H_3	0.009	0.042	0.070	0.028	0.033	0.030	0.843	1.186
C_4	-0.146	-0.065	-0.016	0.049	0.081	0.065	0.604	1.654
H_5	0.002	0.050	0.080	0.030	0.048	0.039	0.618	1.618
C_6	0.047	0.088	0.134	0.046	0.041	0.044	1.122	0.891
C_7	-0.115	-0.072	-0.021	0.052	0.042	0.047	1.227	0.815
H_8	0.010	0.034	0.055	0.021	0.025	0.023	0.831	1.203
C_9	-0.005	0.053	0.067	0.014	0.058	0.036	0.244	4.106
C_{10}	-0.005	0.053	0.067	0.014	0.058	0.036	0.244	4.107
N_{11}	-0.206	-0.161	-0.108	0.053	0.045	0.049	1.175	0.851
C_{12}	-0.025	0.017	0.055	0.037	0.043	0.040	0.871	1.149
H_{13}	0.009	0.042	0.070	0.028	0.033	0.030	0.843	1.186
C_{14}	-0.146	-0.065	-0.016	0.049	0.081	0.065	0.604	1.654
H_{15}	0.002	0.050	0.080	0.030	0.048	0.039	0.618	1.618
C_{16}	0.047	0.088	0.134	0.046	0.041	0.044	1.122	0.891
C_{17}	-0.115	-0.072	-0.020	0.052	0.042	0.047	1.227	0.815
H_{18}	0.010	0.034	0.055	0.021	0.025	0.023	0.831	1.203
O_{19}	-0.153	-0.130	-0.048	0.082	0.023	0.052	3.579	0.279
O_{20}	-0.153	-0.130	-0.048	0.082	0.023	0.052	3.579	0.279
C_{21}	-0.007	0.007	0.030	0.022	0.014	0.018	1.581	0.632
H_{22}	0.029	0.051	0.075	0.024	0.021	0.023	1.145	0.873
H_{23}	0.030	0.043	0.064	0.021	0.013	0.017	1.619	0.618
H_{24}	0.030	0.043	0.064	0.021	0.013	0.017	1.619	0.618
C_{25}	-0.007	0.007	0.030	0.022	0.014	0.018	1.581	0.632
H_{26}	0.029	0.051	0.075	0.024	0.021	0.023	1.145	0.873
H_{27}	0.030	0.043	0.064	0.021	0.013	0.017	1.619	0.618
H_{28}	0.030	0.043	0.064	0.021	0.013	0.017	1.619	0.618

Table 6
Thermodynamic properties (heat capacity, entropy, enthalpy changes, Gibbs free energy, zero-point energy) of Dmobpy1 at temperatures in the range 100-900 K.

Temperature (K)	$C_p{}^0$ (J/mol K)	S_m^0 (J/mol K)	ΔH_m^0 (kJ/mol)	G_{corr} (kJ/mol)	ε_{ZPE} (kJ/mol)
100	92.14	329.01	6.41	556.50	582.97
200	155.64	418.27	19.65	519.01	582.97
300	222.58	497.27	39.36	473.22	582.97
400	288.77	572.90	65.81	419.72	582.97
500	346.42	645.57	98.49	358.81	582.97
600	393.81	714.59	136.41	290.82	582.97
700	432.36	779.57	178.62	216.13	582.97
800	463.99	840.55	224.32	135.14	582.97
900	490.26	897.74	272.90	48.25	582.97

J: Joule, K: Kelvin, C_p^0: Heat capacity, S_m^0: Entropy, ΔH_m^0: Entalphy changes, G_{corr}:Gibbs free energy, ε_{ZPE}: Zero point energy.

dance with the second law of thermodynamics in thermochemical fields according to the relations of thermodynamic parameters [57].

Gibbs free energy (G) is also a critical thermodynamic quantity. G can be defined according to the following formula depending on the temperature (T) and entropy (S):

$$G = H - TS$$

The formula of enthalpy (H) based on internal energy (E) is as follows:

$$H = E + PV$$

In this case, G can be written as:

$$G = E - TS + PV$$

P and V are pressure and volume, respectively. For the solid and liquid phase, the PV value is much lower at atmospheric pressure than the Gibbs free energy, meaning PV can be ignored. Thus, G can be obtained from the formula stated below.

$$G = E - TS$$

The results show that Gibbs free energy gradually decreases with increasing temperature. In other words, entropy and constant volume-specific heat capacity increase, while the calculated values of Gibbs free energy decrease [58].

3.8. Photoluminescence properties

Investigation of the luminescence properties of organic molecules accelerates the development of coordination complexes as potential photoactive materials. because their fluorescent behavior is mainly ligand centered [59].

The solid-state fluorescence spectra of Dmobpy1 was recorded at room temperature and showed in Fig. 9. As displayed in figure the molecule shows an emisssion peak at 507 nm upon excitation at 430 nm. When the emission spectrum of the ligand is examined, the wavelengths where the broad band spectrum is maximum show the green emission band at 507 and 550 nm. The transitions corresponding to these maximum wavelengths are due to the electronic transitions n π^* and π^* π^* absorption [60,61].

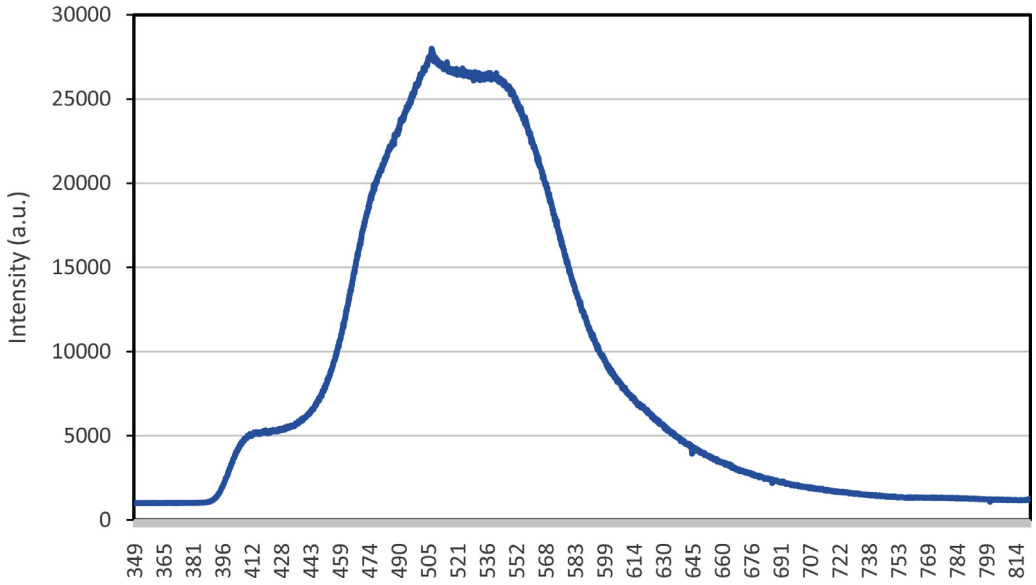

Fig. 9. Experimental Fluorescence emission spectra of Dmobpy1 ligand in solid state.

Table 7
Antimicrobial activity results of Dmobpy1 by Minimum Inhibitory Concentration (MIC) and the inhibition zone diameter (mm).

Microorganisms	Dmobpy1 MIC (μg/ml) [b]	DIZ (mm) [a]	Ampicillin (10 µg) MIC (μg/ml)	DIZ (mm)	Cycloheximide MIC (μg/ml)	DIZ (mm)
S. aureus ATCC 29213	7.81	8.3	-	18.0	-	-
B. thrungiensis ATCC 13367	3.91	10.0	-	-	-	-
L. monocytogenes ATCC 35152	-	-	-	15.1	-	-
P. mirabilis ATCC 29906	-	-	-	12.0	-	-
V. angilarum ATCC43312	-	-	-	12.0	-	-
E. faecalis ATCC 29212	-	-	-	18.2	-	-
E. aerogenes ATCC 51342	-	-	-	18.2	-	-
S.typhimurium ATCC 14028	-	-	-	16.1	-	-
C. tropicalis ATCC M007	-	-	-	16.1	-	18.4
C. parapsilosis ATCC M006	-	-	-	15.3	-	18.1
C. violaceum ATCC 12472 (Diameter of quorum sensing inhibition zone)	-	17.1	3.91	18.1	-	-

MIC (μg/ml): Minimum Inhibitory Concentration
DIZ (mm): Diameter of inhibition zone (mm)
-: No activity observed
c)QS inhibition (radius of pigment inhibition in mm)= radius of growth and pigment inhibition (r_2)-radius of bacterial growth inhibition (r_1).
[a] Not active (–, inhibition zone<5mm); weak activity (5–10mm); moderate activity (10–15mm); strong activity (>15mm).
[b] Not active (–, MIC >500 µg/mL).

3.9. Antimicrobial and antiquorum-sensing activity of compounds

The minimum inhibitory concentration (MIC) of a compound was determined using the microdilution method against nine bacteria (4 Gram-negative and 4 Gram-positive) and two yeast strains Table 7. shows the effects of the compound antimicrobial activity with minimal inhibitory concentration (MIC) and inhibition zone diameter (mm). The title molecule inhibited S. aureus and *B. thrungiensis* with zone of inhibition values ranging from 8.3 mm to -10.0 mm (60 mg/mL). Dmobpy1 demonstrated good activity against *S. aureus* and *B. thrungiensis* with MIC values of 7.81 g/mL and 3.91 g/mL, respectively. Except for S. aureus and B. thuringiensis, no zone of inhibition was observed in other bacteria and yeasts for the compound tested. Indeed, based on these findings, it is possible to conclude that these six bacteria and two yeasts are extremely resistant.

The pathogen bacteria virulence and biofilm feature is controlled by the quorum sensing (QS) system. This system has given new antimicrobial drugs that are effective against antibiotic-resistant bacteria hope. The quorum sensing (QS) system of the bacteria *C. violaceum* ATCC 12472 was used for this test.

In response to the autoinduction known as acly-HSLs, this wild-type bacteria quorum sensing produces violeceum (a purple pigment) [62]. Therefore, drugs that inhibit acly-HSL mediated QS activity in *C. violaceum* will prevent the production of this purple pigment. This inhibition is known as anti-quorum sensing (anti-QS). Therefore, synthesized compounds were examined for their anti-quorum sensing activities against *C. violaceum* ATCC 12472 [63]. The results of inhibition of QS-regulated violeceum production against *C. violaceum* (based on the measurement of the pigment inhibition radius in mm) are presented in Table 7. Dmobpy1 showed strong anti-quorum sensing activity.

3.10. Molecular Docking

Molecular docking is a useful method for calculating the binding affinities of a molecule to a specific receptor of the biological construct. Thanks to this work, we are able to model the interactions between the molecule and the target structure and the stable 3D structure in which the bonds are formed. In particular, it is important to investigate the biological properties of molecular structures and metal complexes for drug design [64,65].

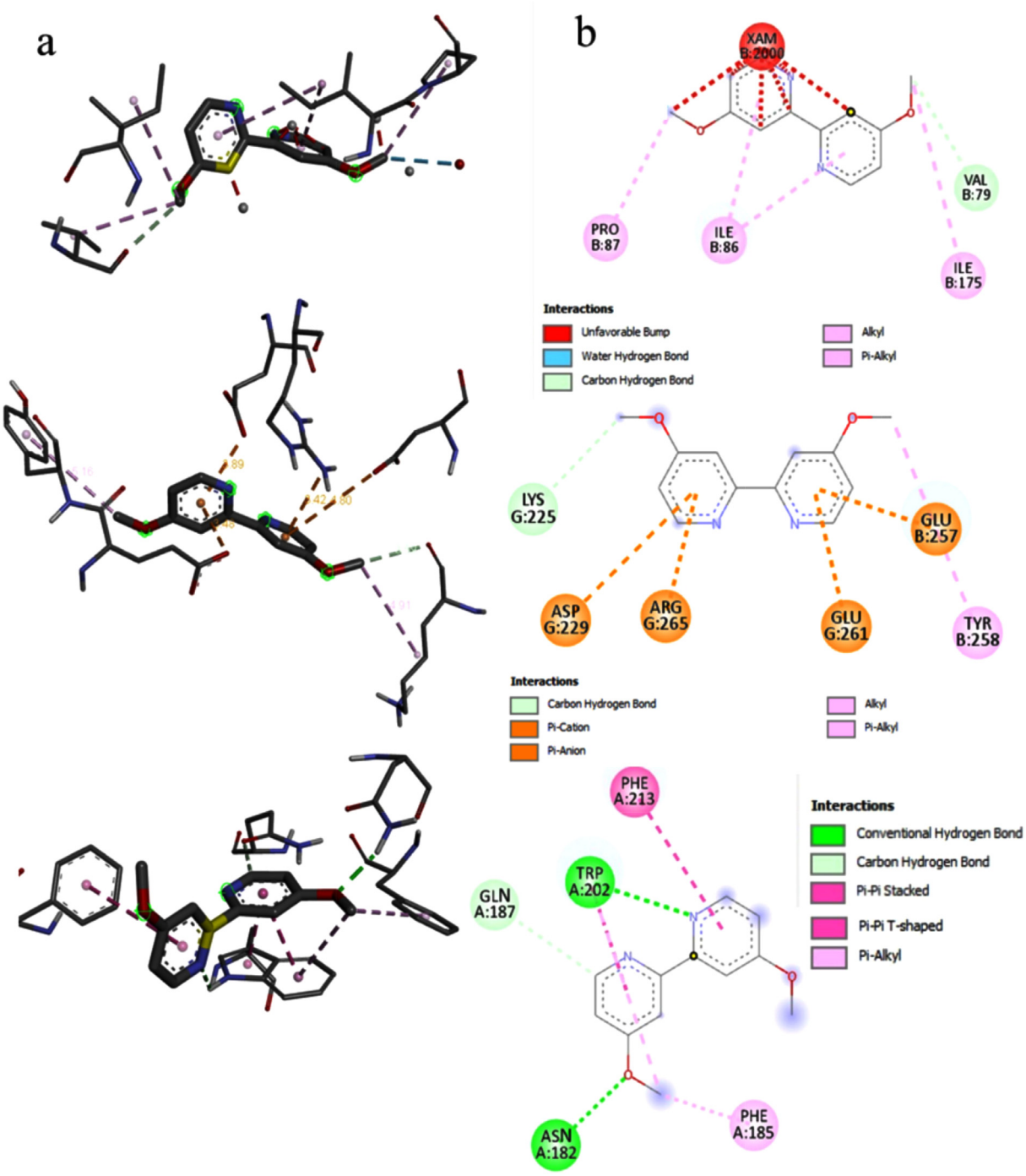

Fig. 10. The molecular docking results of the Dmobpy1 compound with 4URM, 6KOC, and 6GXS proteins, interactions around ligand (a) and 2D forms (b).

The target proteins were selected from structures in which Dmobp1 showed antimicrobial effects.

These three structures were shown in Table 7. The high-resolution structure of 4URM, 6KOC and 6GXS was downloaded from the protein database website (PDB ID: 1YRS) [66] and all molecular docking calculations were performed in Auto Dock-Vina software [67]. T Proteins were made suitable to the docking by removing water molecules and adding polar hydrogens in it and the Kollman charges of the proteins were determined. Auto Dock Tools graphical user interface was used to calculate in whole process. The ligand was theoretically prepared for clamping by minimizing its energy at the B3LYP/6-311++G(d,p) level, and partial charges were calculated with the Geistenger method [68]. The active site of the target proteins which was defined within the grid size of 40 × 40 × 40 Å was bound to the Dmobpy1 molecule by hydrogen bonds. Amongst the docked conformations, one which binded well at the active site was analyzed for detailed interactions in Discover Studio Visualizer 4.0 Software [69]. The stabilized structures due to the interacting of complex structures with residues through some hydrogen-bonding and van der Waals interactions are given in Fig. 10. the best binding mode was determined with −6.2, -6.1 and -5.7 (kcal/mol) energy respectively for 4URM, 6KOC, and 6GXS proteins.

Referring to the Fig. 10, there are hydrogen, Pi-alkyl and alkyl bonds between Dmobpy1 and 4URM protein. Between in the molecule' CH3 group and the O atom of B:VAL:79 is a hydrogen bond with 3.73 Å length. The B:ILE86 and the rings of the Dmobpy1, the Pi-alkyl interactions are about 5.14 and 4.86 Å. The Alkyl interactions with CH3 groups lengths are 4.63 and 4.89 Å.

The title molecule has 1 hydrogen, 1 Pi-Cation and 3 Pi-Anion interactions with the 6KOC protein. The hydrogen bond is between the one of methyl group and the G:LYS225 O atom and its length is 3.59 Å. The ring attached to this methyl group has formed a pi-cation and a pi-anion bond with the protein. The pi-anion interaction is between with the ring and the O atom of the G:ASP229 (4.80 Å).The other bond pi-cation is about 3.42 Å with G:ARG265 of NH. The other ring of the Dmobpy1 has two pi-anion interactions with O atom of the G:GLU261 (3.89 Å) and B:GLU257(3.48 Å). The carbon atom of the methyl group has pi-alkyl bond with A:PHE185(5.20 Å).

There are one conventional and one carbon hydrogen bond with the 6GXS protein. One of the conventional bonds are between the N atom of the pyridine ring and A:TRP202(3.29 Å) and the other one is between the O atom and A:ASN182(2.60 Å).

4. Conclusion

A systematic study has been performed on the structural and spectral characteristics of 4,4′-dimethoxy-2,2′-bipyridine molecule by using experimental spectroscopic methods and quantum chemical calculations. The title molecule was obtained from Sigma Aldrich Chemical Company. The molecular geometry and vibrational wavenumbers of the ligand molecule has been calculated using DFT/B3LYP level with 6-311++G(d,p) basis set. The calculated bond length and bond angle values are in very good agreement with the experimental XRD values. However, small deviations are observed in the harmony between the theoretical and experimental ones. FT-IR and FT-Raman spectra of the molecule are experimentally recorded and analyzed. The calculated vibrational frequencies of the title molecule have been found in good agreement with IR and Raman experimental data. This shows that the obtained structure is very close to the real structure of Dmobpy1. The HOMO–LUMO energy gap is calculated to be 4,99 eV. That is to say, this molecule has a high kinetic stability, and low chemical reactivity. It is determined by MEP analysis that the electron the charge density of the molecule. Apparently, all of the analyzed thermodynamic parameters show an increase in line with the temperature while G is observed to decrease with T, which is due to the rise of molecular vibrations with temperature rise. The bonding ability of the atoms was investigated by calculating the charge distribution, molecular electrostatic potential and Fukui functions of the optimized structure. The maximum value of electrophilic reactivity identifiers was determined in the O_{19} and O_{20} atoms for the Dmobpy1 molecule. Also, the calculated electrophilicity ($\boldsymbol{\omega}$) value showed that the molecule is biologically active.

Antimicrobial applications of Dmobpy1 have been studied against eight and two yeasts. The synthesized compound has weak activity and moderate antimicrobial activity against the two bacteria tested. The compound demonstrated strong anti-quorum sensing activity. The findings suggest that Dmobpy1 has antimicrobial and anti-quorum sensing properties, and that new powerful antimicrobial drugs may be useful in the treatment of bacteria resistant to bacterial infections in the future. A docking study was performed with the protein selected from the structures in which the Dmobpy1 molecule showed biological activity. Based on insertion studies using the 4URM, 6KOC and 6GXS proteins, we have examined in detail the mechanism of the biologically active properties of the title compound.

Declaration of Competing Interest

None

CRediT authorship contribution statement

Meryem Alp: Formal analysis, Writing – original draft, Data curation. **Senay Yurdakul:** Conceptualization, Writing – review & editing, Supervision. **Belgin Erdem:** Investigation, Methodology, Writing – original draft, Writing – review & editing, Resources.

Acknowledgement

This research did not receive any specific grant from funding agencies in the public, commercial, or not-for-profit sectors.

References

[1] G. Cristalli, P. Franchetti, E. Nasini, S. Vittori, M. Grifantini, A. Barzi, E. Lepri, S. Ripa, Metal (II) complexes of 2, 2′-bipyridyl-6-carbothioamide as anti-tumor and anti-fungal agents, European journal of medicinal chemistry 23 (1988) 301–305.
[2] R.S. Kumar, K. Sasikala, S. Arunachalam, DNA interaction of some polymer–copper (II) complexes containing 2, 2′-bipyridyl ligand and their antimicrobial activities, Journal of inorganic biochemistry 102 (2008) 234–241.
[3] A.E. Ozel, S. Kecel, S. Akyuz, Vibrational analysis and quantum chemical calculations of 2, 2′-bipyridine Zinc (II) halide complexes, J. Mol. Struct. 834 (2007) 548–554.
[4] C.C. Scarborough, K. Wieghardt, Electronic Structure of 2,2 -Bipyridine Organotransition-Metal Complexes. Establishing the Ligand Oxidation Level by Density Functional Theoretical Calculations, Inorg. Chem. 50 20 (2011) 9773–9793.
[5] M.I.F. Barbosa, R.S. Corrêa, K.M. de Oliveira, C. Rodrigues, J. Ellena, O.R. Nascimento, V.P.C. Rocha, F.R. Nonato, T.S. Macedo, J.M. Barbosa-Filho, M.B.P. Soares, A.A. Batist, Antiparasitic activities of novel ruthenium/lapachol complexes, Journal of Inorganic Biochemistry 136 (2014) 33–39.
[6] L.J. Yang, Q.L. Liu, M.X. Wang, L.S. Gu, Y.H. Luo, B.W. Sun, Complexation of different transition metals with 4,4-dimethyl-2,2-bipyridine: crystal structure, UV spectra and Hirshfeld surfaces, Spectrochim. Acta A. 166 (2016) 1–7.
[7] Ö. Tamer, H. Mahmoody, K.F. Feyzioğlu, O. Kılınç, D. Avcı, O. Orun, N. Dege, Y. Atalay, Synthesis of the first mixed ligand Mn (II) and Cd (II) complexes of 4-methoxy-pyridine-2-carboxylic acid, molecular docking studies and investigation of their antitumor effects in vitro, Appl Organometal Chem (2019) 5416.
[8] M. Gratzel, Artificial photosynthesis: Water cleavage into hydrogen and oxygen by visible light, Acc. Chem. Res. 14 (1981) 376–384.
[9] S. Aghazada, P. Gao, A. Yella, G. Marotta, T. Moehl, J. Teuscher, J.E. Moser, F.D. Angelis, M. Gratzel, M.K. Nazeeruddin, Ligand engineering fort he efficient dye-sensitized solar cells with Ruthenium sensitizers and Cobalt electrolytes, Inorganic Chemistry 55 13 (2016) 6653–6659.
[10] A. Casini, M.C. Diawara, R. Scopelliti, S.M. Zakeeruddin, M. Gratzel, P.J. Dyson, Synthesis, characterisation and biological properties of gold(III) compounds with modified bipyridine and bipyridylamine ligands, Dalton Trans 39 (2010) 2239–2245.
[11] S. Premkumar, A. Jawahar, T. Mathavan, M.K. Dhas, V.G. Sathe, A.M.F. Benial, DFT calculation and vibrational spectroscopic studies of 2-(tert-butoxycarbonyl (Boc)-amino)-5-bromopyridine, Spectrochimica Acta Part A: Molecular and Biomolecular Spectroscopy 129 (2014) 74–83.
[12] S. Premkumar, T.N. Rekha, R.M. Asath, T. Mathavan, A.M.F. Benial, Vibrational spectroscopic, molecular docking and density functional theory studies on 2-acetylamino-5-bromo-6-methylpyridine, European Journal of Pharmaceutical Sciences 82 (2016) 115–125.
[13] B.Y. Saito, J. Takemoto, B. Hutchinson, K. Nakamoto, Infrared studies of coordination compounds containing low-oxidation- state metals. I. Tris(2,2'-bipyridine) and tris(1,l0-phenanthroline) complexes, Inorg. Chem. 11 (1972) 2003–2011.
[14] V. Amani, N. Safari, H.R. Khavasi, Synthesis, characterization and crystal structure determination of iron(III) hetero-ligand complexes containing 2,20-bipyridine, 5,50-dimethyl-2,20-bipyridine and chloride, [Fe(bipy)Cl4][bipy$H] and [Fe(dmbipy)2Cl2][FeCl4], Polyhedron 26 (2007) 4257–4262.
[15] S.M. Mobin, A.K. Saini, V. Mishra, A. Chaudhary, A series of new heteroleptic Hg(II) complexes: synthesis, crystal structures, and photophysical properties, Polyhedron 110 (2016) 131–141.
[16] Y. Kusano, K. Ohno, T. Fujihara, Crystal structure of 4,4′-dimethoxy-2,2′-Bipyridine, Crystallographic Communications 71 (2015) 623–624.
[17] S.N. Sovari, F. Zobi, Recent Studies on the Antimicrobial Activity of Transition Metal Complexes of Groups 6–12, Chemistry 2 (2) (2020) 418–452.
[18] R. Kaushal, N. Kumar, P. Awasthi, K. Nehra, Syntheses, characterization, and antibacterial study of titanium complexes, Turkish Journal of Chemistry 37 (2013) 936–945.

[19] NCCLS 2003, Performance Standards for Antimicrobial Susceptibility Testing:13th Informational Supplement (Disk Diffusion Supplemental Tables). NCCLS document M100-S13 (M2), supplement to NCCLS document M2-A8 (disk diffusion).
[20] K.H. McLean, M.K. Winson, L. Fish, A. Taylor, S.R. Chhabra, M. Camara, M. Daykin, J.H. Lamb, S. Swift, B.W. Bycroft, G.S. Stewart, P. Williams, Quorum sensing and Chromobacterium violaceum: exploitation of violacein production and inhibition for the detection of N-acyl homoserine lactones, Microbiology 143 (1997) 3703–3711.
[21] NCCLS 2000, Performance Standards for Antimicrobial Susceptibility Testing: 10th Informational Supplement (Aerobic Dilution, MIC Testing Supplemental Tables. NCCLS document M100-S10(M7), supplement to NCCLS document M7-A5 (MIC testing).
[22] M.J. Frisch, G.W. Trucks, H.B. Schlegel, G.E. Scuseria, M.A. Robb, J.R. Cheeseman, G. Scalmani, V. Barone, B. Mennucci, G.A. Petersson, H. Nakatsuji, M. Caricato, X. Li, H.P. Hratchian, A.F. Izmaylov, J. Bloino, G. Zheng, J.L. Sonnenberg, M. Hada, M. Ehara, K. Toyota, R. Fukuda, J. Hasegawa, M. Ishida, T. Nakajima, Y. Honda, O. Kitao, H. Nakai, T. Vreven, J.A. Montgomery Jr., J.E. Peralta, F. Ogliaro, M. Bearpark, J.J. Heyd, E. Brothers, K.N. Kudin, V.N. Staroverov, R. Kobayashi, J. Normand, K. Raghavachari, A. Rendell, J.C. Burant, S.S. Iyengar, J. Tomasi, M. Cossi, N. Rega, J.M. Millam, M. Klene, J.E. Knox, J.B. Cross, V. Bakken, C. Adamo, J. Jaramillo, R. Gomperts, R.E. Stratmann, O. Yazyev, A.J. Austin, R. Cammi, C. Pomelli, J.W. Ochterski, R.L. Martin, K. Morokuma, V.G. Zakrzewski, G.A. Voth, P. Salvador, J.J. Dannenberg, S. Dapprich, A.D. Daniels, Ö. Farkas, J.B. Foresman, J.V. Ortiz, J. Cioslowski, D.J. Fox, Gaussian 09, Gaussian, Inc., Wallingford CT, 2009.
[23] R. Dennington II, T. Keith, J. Millam, K. Eppinett, W.L. Hovell, R. Gilliland, GaussView, Version 3.09, Semichem, Shawnee Mission, KS, 2003.
[24] A.D. Becke, Density-functional thermochemistry. III. The role of exact Exchange, J. Chem. Phys. 98 (1993) 5648–5652.
[25] C. Lee, W. Yang, R.G. Parr, Development of the Colle-Salvetti correlation-energy formula into a functional of the electron density, Phys. Rev. B. 37 (1988) 785–789.
[26] M.U. Munshi, J. Martens, G. Berden, J. Oomens, Vibrational Spectra of the Ruthenium−Tris-Bipyridine Dication and Its Reduced Form in Vacuo, J. Phys. Chem. A 124 (2020) 2449–2459.
[27] P.J. Merrick, D. Moran, L. Radom, An Evaluation of Harmonic Vibrational Frequency Scale Factors, J. Phys. Chem. A 111 (2007) 11683–11700.
[28] S. Eğlence-Bakır, S. Celik, M. Şahin, A.E. Ozel, S. Akyuz, B. Ülküseven, Synthesis, molecular modelling, FT-IR, Raman and NMR characterization, molecular docking and ADMET study of new nickel(II) complex with an N4-tetradentate thiosemicarbazone, Journal of Biomolecular Structure and Dynamics (2020), doi:10.1080/07391102.2020.1775128.
[29] Ö. Tamer, D Avcı, N. Dege, Y. Atalay, Synthesis, crystal structure, photophysical properties, density functional theory calculations and molecular docking studies on Cd(II) complex of 4,4′-dimethyl-2,2′-dipyridyl, Journal of Molecular Structure (2020).
[30] J. Prasshanth, B.V. Reddy, G.R. Rao, Investigation of torsional potentials, molecular structure, vibrational properties, molecular characteristics and NBO analysis of some bipyridines using experimental and theoretical tools, J. Mol. Struct. (2016).
[31] N. Boukabcha, A. Djafri, Y. Megrouss, Ö. Tamer, D. Avcı, M. Tuna, N. Dege, A. Chouaih, Y. Atalay, A. Djafri, F. Hamzaoui, Synthesis, crystal structure, spectroscopic characterization and nonlinear optical properties of (Z)-N'-(2,4-dinitrobenzylidene)-2-(quinolin-8-yloxy) acetohydrazide, Journal of Molecular Structure 1194 (2019) 112–123.
[32] J.K. Ojha, B.V. Reddy, G.R. Rao, Vibrational analysis and valence force field for nitrotoluenes, dimethylanilines and some substituted methylbenzenes, Spectrochim. Acta A. 96 (2012) 632–643.
[33] E. Akalin, S. Celik, S. Akyuz, Molecular modeling, dimer calculttons, vibrational spectra and molecular docking studies of 5-Chlorouracil, J. of Applied Spectroscopy 86 (2020) 6.
[34] R. Thomas, Y. Sheena Mary, K.S. Resmi, B. Narayana, S.B.K. Sarojini, S. Armaković, S.J. Armaković, G. Vijayakumar, C. Van Alsenoy, B.J. Mohan, Synthesis and spectroscopic study of two new pyrazole derivatives with detailed computational evaluation of their reactivity and pharmaceutical potential, J. Mol. Struct. 1181 (2019) 599–612.
[35] L. Ravindranath, B.V. Reddy, Theoretical and experimental study of torsional potentials, molecular structure (monomer and dimer), vibrational analysis and molecular characteristics of some dimethyl bipyridines, J. Mol. Struct. 1200 (2020) 127089.
[36] Y. Erdogdu, T.R. Sertbakan, M.T. Güllüoğlu, Ş. Yurdakul, A. Güvenir, FT-IR and Raman Spectroscopy and Computation of 5-Methylfurfural, Journal of Applied Spectroscopy 85 (3) (2018) 517–525.
[37] Y. Erdogdu, Ö. Dereli, E.K. Sarıkaya, Vibrational (FT-IR and FT-Raman), NMR and quantum chemical investigations on 7-Methylcoumarin, Journal of Spectroscopy and Molecular Sciences 2 (2020) 51–64.
[38] A. Atilgan, S. Yurdakul, Y. Erdogdu, M.T. Güllüoglu, DFT simulation, quantum chemical electronic structure, spectroscopic and structure-activity investigations of 4-acetylpyridine, J. Mol. Struct. 1161 (2018) 55–65.
[39] S. Subashchandrabose, A.R. Krishnan, H. Saleem, V. Thanikachalam, G. Manikandan, Y. Erdogdu, FT-Raman FT-IR, NMR spectral analysis and theoretical NBO, HOMO–LUMO analysis of bis (4-amino-5-mercapto-1, 2, 4-triazol- 3-yl) ethane by ab initio HF and DFT methods, J. Mol. Struct. 981 (1–3) (2010) 59–70.
[40] Y.S. Mary, Y.S. Mary, K.S. Resmi, R. Thomas, DFT and molecular docking investigations of oxicam derivatives, Heliyon 5 (7) (2019) 02175.
[41] S.M. Soliman, M. Hagar, F.S.H. El Ashry, Synthesis of two new silver(I) complexes with 3-bromoquinoline: Molecular structure, spectroscopic characterizations and DFT studies, Spectrochim. Acta 145 (2015) 270–279.
[42] R.J. Parr, L.V. Szentpaly, S. Liu, Electrophilicity Index, J. Am. Chem. Soc. 121 (1999) 1922–1924.
[43] L. Tan, S. Zhang, X. Liu, Y. Chen, X. Liu, Experimental and density functional theory (DFT) studies on the DNA-binding trend and spectral properties of two new Ru(II) complexes: [Ru(L)2(mip)](ClO4)2 (L=2,9-dmp and 4,7-dmp), Journal of Organometallic Chemistry 693 (2008) 3387–3395.
[44] S. Celik, M. Alp, S. Yurdakul, A combined experimental and theoretical study on vibrational spectra of 3-pyridyl methyl ketone, Spectroscopy Letters 53 (4) (2020) 234–248.
[45] F.J. Luque, J.M. Lopez, M. Orozco, Perspective on "Electrostatic interactions of a solute with a continuum. A direct utilization of ab initio molecular potentials for the prevision of solvent effects", Theor. Chem. Acc. 103 (200) (1981) 343–345.
[46] S. Çelik, S. Basoğlu, Ş. Yurdakul, Vibrational spectroscopic and density functional study on 1,2,4-triazolo-[1,5-a]pyrimidine, Vibrational spectroscopy 92 (2017) 280–286.
[47] J. George, J.C. Prasana, S. Muthu, T.K. Kuruvilla, S. Sevanthi, R.S. Saji, Spectroscopic (FT-IR, FT Raman) and quantum mechanical study on N-(2,6-dimethylphenyl)-2-{4-[2-hydroxy-3-(2-methoxyphenoxy)propyl]piperazin-1-yl}acetamide, J. Mol. Struct. 1171 (2018) 268–278.
[48] N.M. O'Boyle, A.L. Tenderholt, K.M. Langner, cclib: A library for package-independent computational chemistry algorithms, Journal of Computational Chemistry 29 (2019) 839–845.
[49] P. Politzer, J.S. Murray, Molecular Electrostatic Potentials and Chemical Reactivity, Reviews in Computational Chemistry 2 (1991).
[50] E. Scrocco, J. Tomasi, Topics in Current Chemistry, vol. 42, Verlag, Springer, Berlin, 1973.
[51] X.J. Mao, Atomic Charges in Molecules: A Classical Concept in Modern Computational Chemistry, Journal of Postdoctoral Research 2 (2014) 2.
[52] F. De Proft, C. Van Alsenoy, A. Peeters, W. Langenaeker, P. Geerlıngs, Atomic Charges, Dipole Moments, and Fukui Functions Using the Hirshfeld Partitioning of the Electron Density, Journal of Computational Chemistry 23 (2002) 1198–1209.
[53] P. Bultinck, R. Carbo-Dorca, W. Langenaeker, Negative Fukui functions: New insights based on electronegativity equalization, J. Chem. Phys. 118 (2003) 4349.
[54] W. Yang, W.J. Mortier, The Use of Global and Local Molecular Parameters for the Analysis of the Gas-Phase Basicity of Amines, J. Am. Chem. Soc. 108 (1986) 5708–5711.
[55] R.G. Parr, W. Yang, Density Functional Approach to the Frontier-Electron Theory of Chemical Reactivity, J. Am. Chem. Soc. 106 (1984) 4049–4050.
[56] R.K. Roy, S. Krishnamurti, P. Geerlings, S. Pal, Local Softness and Hardness Based Reactivity Descriptors for Predicting Intra- and Intermolecular Reactivity Sequences: Carbonyl Compounds, J. Phys Chem A 102 (1998) 3746–3755.
[57] A. Hellal, D. Rachida, S. Zaout, M. Elkolli, S. Chafaa, L. Touafri, N. Chafai, M. Mehri, K. Benbougerra, Structural, Electronic, Vibrational, Optical and Thermodynamic Properties of 3-Oxo-3-p-tolylpropylphosphonic Acid and 4-Oxo-4-ptolyl-butyric Acid: Density Functional Theory Study, J. Mol. Struct. 1171 (2018) 527–540.
[58] fJ. Liu, H. Han, X. Zhang, S. Li, S. Ge, G. Zhang, T. Gao, First-Principles Study the Structural, Electronic, Vibrational and Thermodynamic Properties of Zr1-HfxCoH3, International Journal of Hydrogen Energy 43 (2018) 19152–19163.
[59] X. Zhang, N. Xing, F. Bai, L. Wan, H. Shan, Y. Hou, Y. Xing, Z. Shic, Multi-functional d10 metal–organic materials based on bis-pyrazole/pyridine ligands supported by a 2,6-di(3-pyrazolyl)pyridine with different spanning flexible dicarboxylate ligands: synthesis, structure, photoluminescent and catalytic properties, Cryst. Eng. Comm. 15 (2013) 9135–9147.
[60] X. Feng, Y. Feng, J.J. Chen, S.W. Ng, L.Y. Wang, J.Z. Guo, Reticular three-dimensional 3d-4f frameworks constructed through substituted imidazole-dicarboxylate: syntheses, luminescence and magnetic properties study, Dalton Trans 44 (2015) 804.
[61] U. Balijapalli, M. Tanaka, M. Auffray, C.Y. Chan, Y.T. Lee, Y. Tsuchiya, H. Nakanotani, C. Adachi, Utilization of Multi-Heterodonors in Thermally Activated Delayed Fluorescence Molecules and Their High Performance Bluish-Green Organic Light-Emitting Diodes, ACS Appl. Mater. Interfaces 12 (2020) 9498–9506.
[62] X. Zhao, Z. Yu, T. Ding, Quorum-Sensing Regulation of Antimicrobial Resistance in Bacteria, Microorganisms 8 (3) (2020) 425.
[63] T.B. Rasmussen, M. Givskov, Quorum-sensing inhibitors as anti-pathogenic drugs, Int. J. Med. Microbiol. 296 (2006) 149–161.
[64] D. Avcı, S. Altürk, F. Sönmez, Ö. Tamer, A. Başoğlu, Y. Atalay, B. Zengin Kurt, Synthesis, DFT calculations and molecular docking study of mixed ligand metal complexes containing 4,40-dimethyl-2,20-bipyridyl as aglucosidase inhibitors, J. of Mol. Struct. 1205 (2020) 127655.
[65] N. Dege, Ö. Özge, D. Avcı, A. Başoğlu, F. Sönmez, M. Yaman, Ö. Tamer, Y. Atalay, B. Zengin Kurt, Concentration effects on optical properties, DFT, crystal characterization and a-glucosidase activity studies: Novel Zn(II) complex, Spectrochim ACTA A 262 (2021) 120072.
[66] https://www.rcsb.org/.
[67] O. Trott, A.J. Olson, AutoDock Vina: improving the speed and accuracy of docking with a new scoring function, efficient optimization, and multithreading, Journal of computational chemistry 31.2 (2010) 455–461.

[68] S. Parveen, M.A. Al-Alshaikh, C.Y. Panicker, A.A. El-Ermam, B. Narayana, V. Saliyan, B.K. Sarojini, C.V. Alsenoy, Vibrational and structural observations and molecular docking study on 1-{3-(4-chlorophenyl)-5-[4-(propan-2-yl)phenyl]-4,5-dihydro-1H-pyrazol-1-yl}-ethanone, J. Mol. Struct. 1112 (2016) 136–146.

[69] BIOVIADassault Systèmes, Discovery Studio Visualizer Software, Version 4.0, Dassault Systèmes, San Diego, 2021.